



HAL
open science

Synthesis and crystallographic investigation of dicobalt tetrahedrane complexes ligated by 2-butyne-1,4-diol. In silico evaluation of their efficiency as anticancer metallodrugs

Ahmed Said Mohamed, Isabelle Jourdain, Michael Knorr, Stephanie Befly, Abdirahman Elmi, Farhan Siddique, Samir Chtita, Carsten Strohmann, Annika Schmidt, Mostafa Hussien

► To cite this version:

Ahmed Said Mohamed, Isabelle Jourdain, Michael Knorr, Stephanie Befly, Abdirahman Elmi, et al.. Synthesis and crystallographic investigation of dicobalt tetrahedrane complexes ligated by 2-butyne-1,4-diol. In silico evaluation of their efficiency as anticancer metallodrugs. *Journal of Molecular Structure*, 2025, 1321 (4), pp.140108. 10.1016/j.molstruc.2024.140108 . hal-04703542

HAL Id: hal-04703542

<https://hal.science/hal-04703542v1>

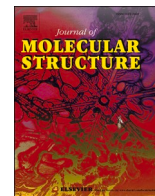
Submitted on 27 Sep 2024

HAL is a multi-disciplinary open access archive for the deposit and dissemination of scientific research documents, whether they are published or not. The documents may come from teaching and research institutions in France or abroad, or from public or private research centers.

L'archive ouverte pluridisciplinaire **HAL**, est destinée au dépôt et à la diffusion de documents scientifiques de niveau recherche, publiés ou non, émanant des établissements d'enseignement et de recherche français ou étrangers, des laboratoires publics ou privés.



Distributed under a Creative Commons Attribution 4.0 International License



Synthesis and crystallographic investigation of dicobalt tetrahedrane complexes ligated by 2-butyne-1,4-diol. *In silico* evaluation of their efficiency as anticancer metallodrugs

Ahmed Said Mohamed^{a,b,*}, Isabelle Jourdain^{b,*}, Michael Knorr^{b,*}, Stephanie Befly^b, Abdirahman Elmi^a, Farhan Siddique^{c,d}, Samir Chtita^e, Carsten Strohmann^f, Annika Schmidt^f, Mostafa A. Hussien^{g,h}

^a Institut de Recherche Médicinale, Centre d'Etude et de Recherche de Djibouti, IRM-CERD, Route de l'Aéroport, Djibouti, Djibouti

^b Université de Franche-Comté, Institut UTINAM UMR CNRS 6213, 16 Route de Gray, F-25030 Besançon, France

^c School of Pharmaceutical Science and Technology, Tianjin University, Tianjin 300072 PR China

^d Department of Pharmaceutical Chemistry, Faculty of Pharmacy, Bahaaddin Zakariya University, Multan 60800 Pakistan

^e Laboratory of Analytical and Molecular Chemistry, Faculty of Sciences Ben M'Sik, Hassan II University of Casablanca, B.P. 7955 Sidi Othmane, Casablanca, Morocco

^f Technische Universität Dortmund, Anorganische Chemie, Otto-Hahn-Strasse 6, D-44227 Dortmund, Germany

^g Department of Chemistry, Faculty of Science, King Abdulaziz University, Jeddah, Saudi Arabia

^h Department of Chemistry, Faculty of Science, Port Said University, Port Said, 42521, Egypt

ARTICLE INFO

Keywords:

Dicobalt tetrahedranes
Crystal structure
Hydrogen bonding
Anticancer metallodrugs
Molecular docking

ABSTRACT

A series of dicobalt carbonyl dimetallatetrahedranes of type $[\text{Co}_2(\text{CO})_4\text{L}_2(\mu\text{-HOCH}_2\text{C}\equiv\text{CCH}_2\text{OH})]$ ($\text{L} = \text{CO}, \text{P}(\text{OR})_3$; $\text{L}_2 = \text{Ph}_2\text{PN}(\text{H})\text{PPh}_2, \text{Ph}_2\text{PN}(\text{Me})\text{PPh}_2, \text{Ph}_2\text{PCH}_2\text{PPh}_2$), ligated by 1,4-butanediol (BUD) was synthesized and structurally characterized at 100 K by single-crystal X-ray diffraction to analyze in addition to the molecular architectures their propensity to generate intra- and intermolecular secondary interactions. For several selected examples, also Hirshfeld surface analyses have been performed. To evaluate the replacement of OH vs. SR, this series of BUD-based dimetallatetrahedranes (1-3) was completed by the preparation of the structurally related complexes $[\text{Co}_2(\text{CO})_4\text{L}_2(\mu\text{-RSCH}_2\text{C}\equiv\text{CCH}_2\text{SR})]$ (4-5). The crystallographically characterized complex $[\text{Co}_2(\text{CO})_4\{\text{P}(\text{OPh})_3\}_2(\mu\text{-}t\text{-BuSCH}_2\text{C}\equiv\text{CCH}_2\text{SBu-}t)]$ (4) was obtained in a Nicholas-type reaction between $[\text{Co}_2(\text{CO})_4\{\text{P}(\text{OPh})_3\}_2(\mu\text{-HOCH}_2\text{C}\equiv\text{CCH}_2\text{OH})]$ (2a) and *t*-BuSH. Alternatively, the latter series 4-5 was obtained in much improved yield by direct treatment of $[\text{Co}_2(\text{CO})_6\text{L}_2]$ with the thioether-functionalized alkynes $\text{RSCH}_2\text{C}\equiv\text{CCH}_2\text{SR}$ ($\text{R} = t\text{-Bu}, \text{Ph}, \text{Bz}$). The experimental crystallographic data were compared with those obtained by DFT computing. The anticancer capacity of this series of compounds was evaluated against prostate, breast and liver cancers through *in silico* docking simulations. Some compounds displayed docking scores against prostate, breast, and liver cancer proteins in the range between -4.91 – -11.01 kcal/mol, indicating a potential as bimetallic metallodrugs in cancer therapy, deserving more detailed *in vitro* investigations.

1. Introduction

The cytotoxicity and other side effects of traditional platinum-based anticancer drugs such as cisplatin or oxaliplatin has compelled researchers to investigate the biological activity of other transition metal-based compounds as alternatives [1,2]. Among them, cobalt-based metallodrugs are an emerging class of compounds. Cobalt is an essential trace element in the human metabolism and found in vitamin B12, also known as cobalamin. It plays a role in cell division, contributes to

normal energy metabolism, participates in the formation of red blood cells and the functioning of the immune system [3]. This essential element has therefore been used to design many cobalt complexes displaying various promising biological activities [4,5]. In this context, several mononuclear cobalt complexes have been synthesized and evaluated for their anticancer activity. Examples are cobalt(III) complexes based on chelating Schiff bases which display a potential for treatment in cancer chemotherapy [6–13]. A strategy to develop novel bioactive molecules is the incorporation of a metal-metal bonded

* Corresponding authors.

E-mail addresses: demahom0907@live.com (A.S. Mohamed), isabelle.jourdain@univ-fcomte.fr (I. Jourdain), michael.knorr@univ-fcomte.fr (M. Knorr).

<https://doi.org/10.1016/j.molstruc.2024.140108>

Received 12 July 2024; Received in revised form 11 September 2024; Accepted 16 September 2024

Available online 19 September 2024

0022-2860/© 2024 The Author(s). Published by Elsevier B.V. This is an open access article under the CC BY license (<http://creativecommons.org/licenses/by/4.0/>).

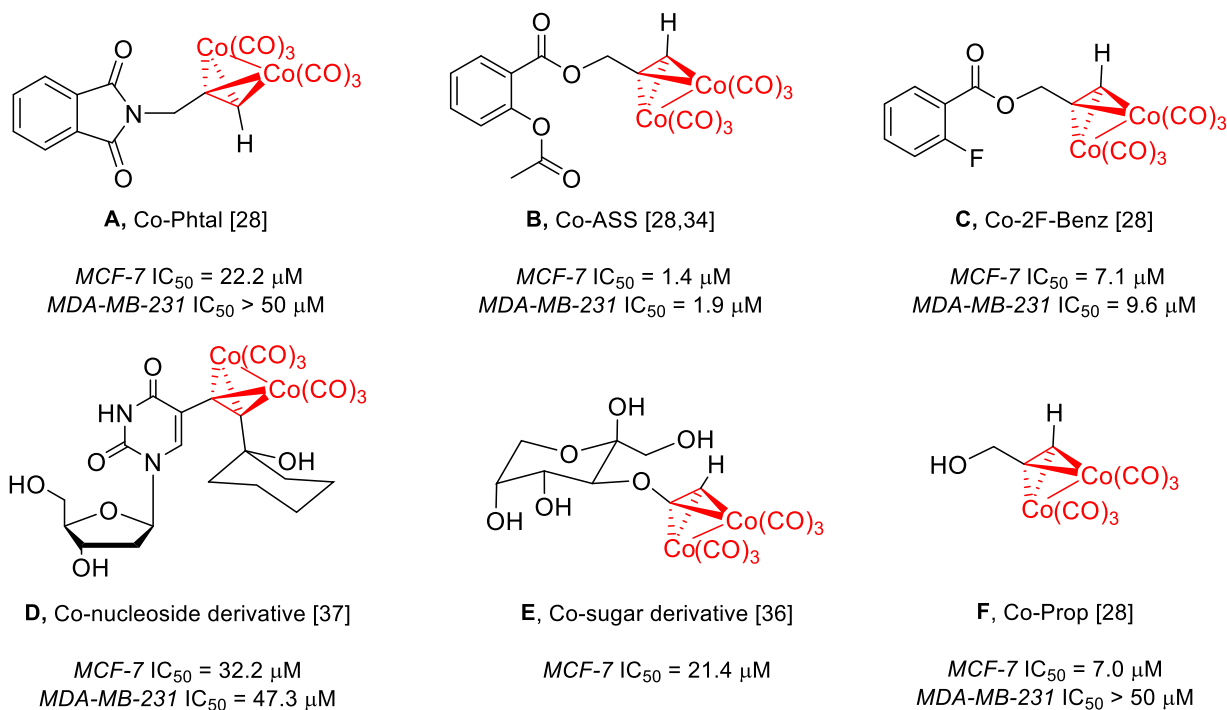
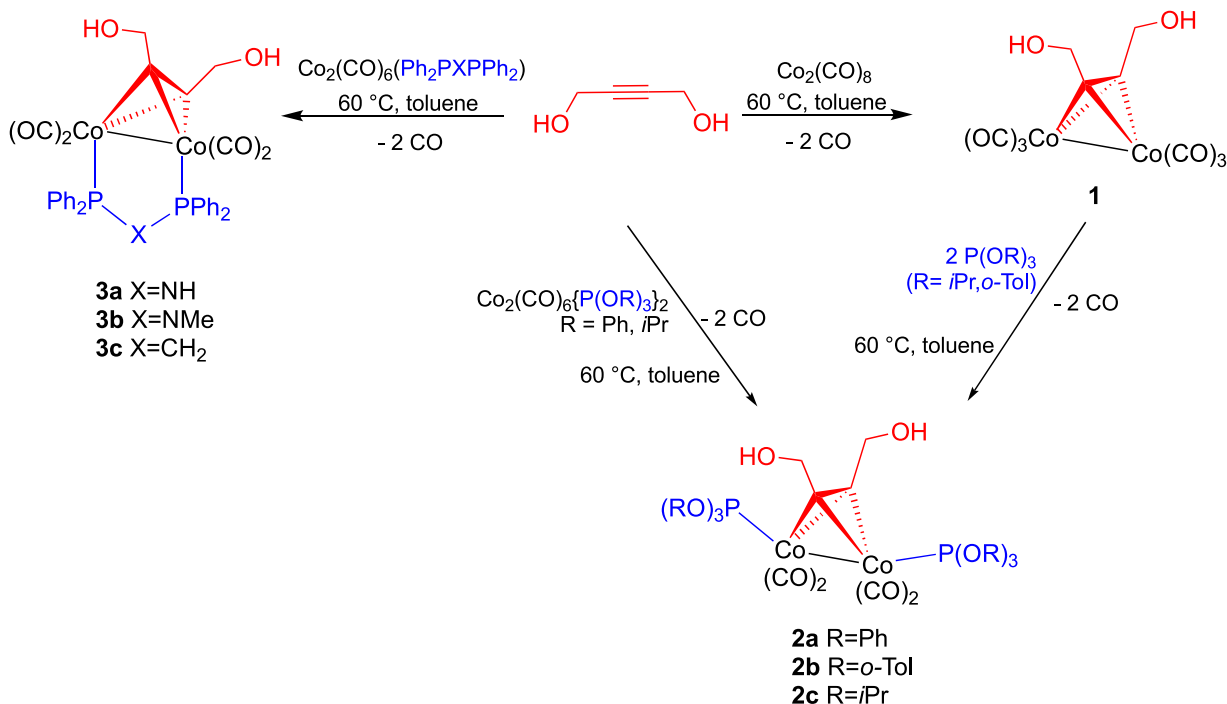


Chart 1. Examples of dicobalt-alkyne complexes with cytotoxic profiles against breast cancer.

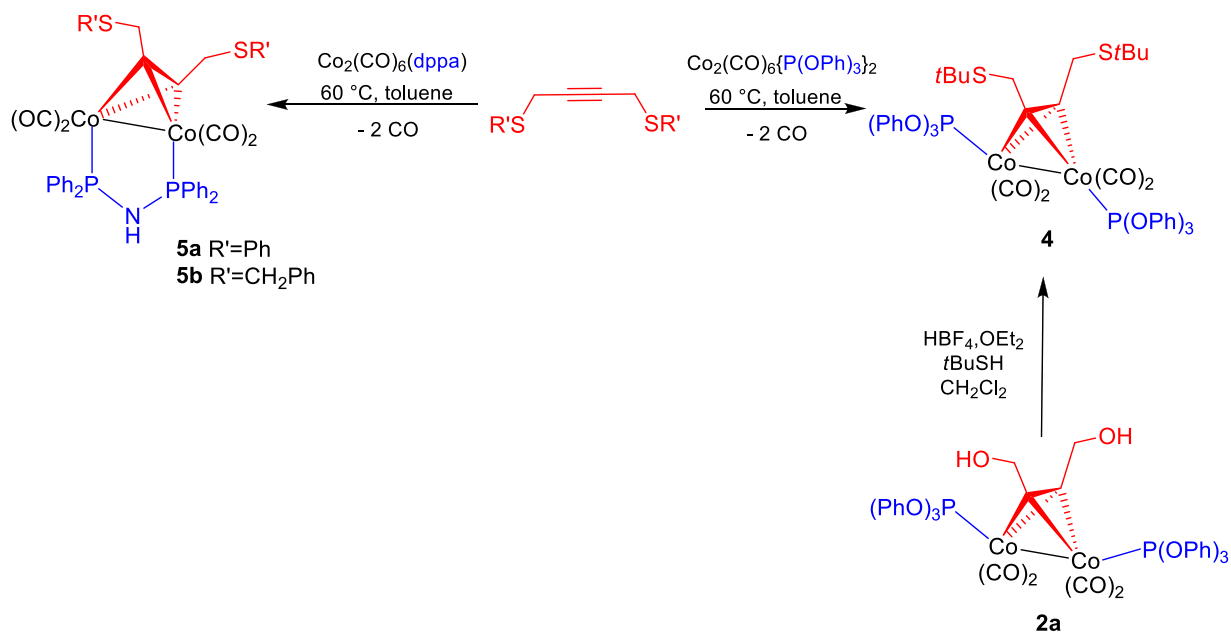
bimetallic scaffold which may provide cooperative effects between the two adjacent metal centers. Such cooperativity is observed in the natural diiron metalloenzyme [FeFe]-hydrogenase to produce H_2 and numerous diiron artificial enzymes have been investigated as well as carbonyl diiron and diruthenium complexes for biological studies [14–18]. Other examples of dinuclear bis(diphenylphosphino)methane-bridged homo- and heterobimetallic complexes bioactive species are referenced in a recent review [19].

In the case of cobalt, dinuclear metal-metal-bonded cobalt carbonyl compounds are known for their catalytic activities such as

hydroformylation, hydrosilylation or as intermediates in the Pauson-Khand reaction [20–23]. This latter reaction implies the formation of dicobalttetrahedranes $[Co_2(CO)_6(\mu-R\equiv CR')]$, formed readily by treatment of dicobalt octacarbonyl with terminal and interne alkynes [24]. The facile synthetic access to these 40-electron clusters has stimulated many research groups to explore their potential for biological and medicinal applications. This encompasses their use as diagnostic agents in the Carbonyl Metallo Immuno Assay (CMIA) or as hormonally active compounds [25–27]. Gust *et al.* reported the reaction of propargyl phthalimide with $[Co_2(CO)_8]$ and determined the cytotoxicity and DNA



Scheme 1. Synthesis of a series of dicobalt 1,4-butyne diol complexes.



Scheme 2. Synthesis of a series of dicobalt $\text{R}'\text{SCH}_2\text{C}\equiv\text{CCH}_2\text{SR}'$ complexes.

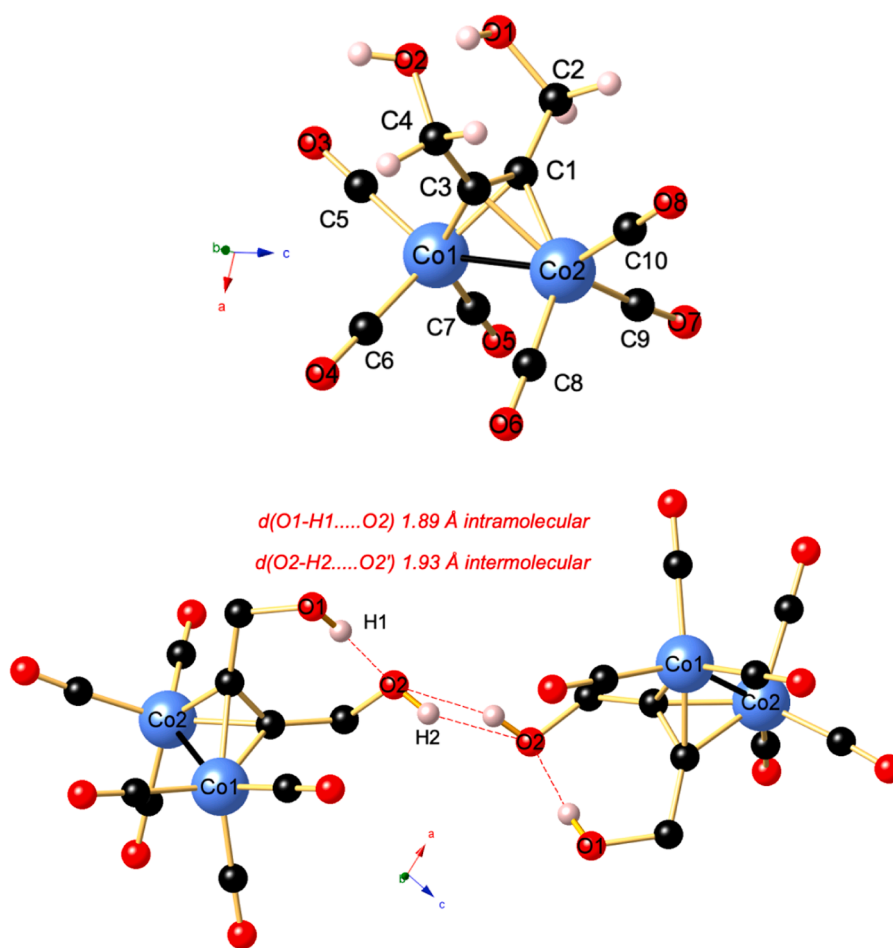


Fig. 1. (Top) Perspective view of **1** showing the atom-labeling scheme. Selected distances (Å) and angles (°). Co1–Co2 2.4750(6), Co1–C1 1.970(3), Co1–C3 1.965(3), Co2–C1 1.950(3), Co2–C3 1.965(3), Co1–C5 1.803(3), Co1–C6 1.827(3), Co1–C7 1.825(3), Co2–C8 1.821(3), Co2–C9 1.827(3), Co2–C10 1.806(3), C1–C3 1.325(4), C1–C2 1.488(4), C3–C4 1.481(4); Co1–C1–Co2 78.31(10), Co1–C3–Co2 78.07(10). (Bottom) View of the dimer of **1** featuring both intra- and intermolecular hydrogen bonding.

Table 1
 $^{31}\text{P}\{^1\text{H}\}$ NMR data and IR (ν)/CO frequencies in solution and in the solid state.

Complex	δ_p ppm (CDCl ₃)	$\nu(\text{CO})$ cm ⁻¹ (CH ₂ Cl ₂)	$\nu(\text{CO})$ cm ⁻¹ (ATR)
1	-	2095, 2056, 2029	2091, 2059, 2020, 1999
2a	152.3	2045, 1991	2046, 2000, 1984, 1969
2b	148.5	2044, 1989	2040, 2003, 1982
2c	157.4	2026, 1966	2021, 1960
3a	96.1	2028, 1998, 1971	2018, 1986, 1957
3b	115.1	2027, 1997, 1970	2018, 1988, 1963, 1942
3c	41.6	2024, 1994, 1986	2019, 2012, 1990, 1956, 1931
4	150.5	2042, 2008, 1986	2045, 2007, 1987, 1967
5a	95.2	2028, 1998, 1972	2020, 1986, 1965, 1945
5b	95.8	2026, 1995, 1970	2017, 1988, 1954, 1937

binding efficiency of the resulting complex *N*-(2-propynyl)phthalimide] hexacarbonyldicobalt (compound **A** of Chart 1) [28,29]. A lot of work has also been devoted to investigate the efficiency of dicobalttetrahedranes as anticancer drugs [8,30–33]. In 1987, Hyama *et al.* mentioned the activity of $[\text{Co}_2(\text{CO})_6(\mu\text{-HCC-C}(\text{OEt})_2\text{-C}(\text{NH}_2)=\text{C}(\text{H})\text{-CO}_2^t\text{Bu})]$ against P388 leukemia cells [34]. Jung *et al.* synthesized and investigated the *in vitro* anticancer activity of a series of dicobalt-alkyne derivatives (dicobalthexacarbonyl-[2-propynylsalicylate], dicobalthexacarbonyl-[(2-propynyl)-2-acetyl salicylate], dicobalthexacarbonyl-[*N*-2-propynyl-benzothiazolidin-3-one-1,1-dioxide], and dicobalthexacarbonyl-[1-(2-chlorophenyl)-1-phenyl-4-pyrrolidinyl-2-butyn-1-ol]) towards 3677 human melanoma and H2981 lung carcinoma cell lines. The screening results revealed an improved activity of the dicobalt-alkyne complexes derived from salicylic acid compared to $\text{Co}_2(\text{CO})_8$, CoCl_2 or the free alkyne ligand [30]. Subsequent screening of various tetrahedranes as cytostatics on further tumor cell lines confirmed the anti-proliferative effects of this class of compounds such as the particular efficient aspirin derivative [(2-propynyl)acetylsalicylate]-hexacarbonyldicobalt (Co-ASS, compound **B** in Chart 1) and its derivatives (compound **C** in Chart 1). Compound **B** was even more active than cisplatin on the two breast cancer cell lines [28]. The mode of action of Co-ASS seems being multifactorial and the design of new derivatives to understand better the variation of anticancer activity is still under

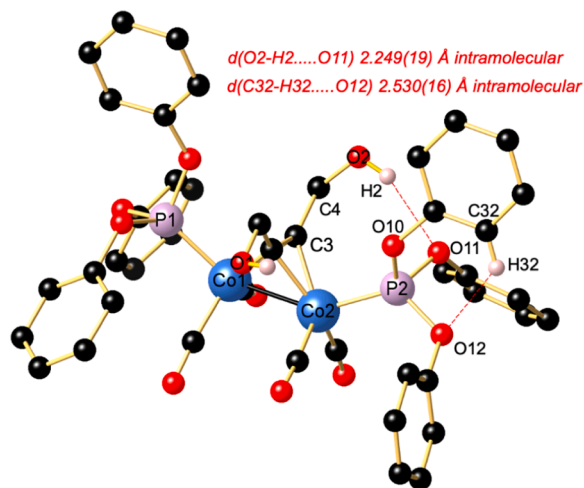


Fig. 2. Perspective view of **2a** showing the atom-labeling scheme. Hydrogen atoms have been omitted for clarity. Selected distances (Å) and angles (°). Co1–Co2 2.4588(17), Co1–P1 2.1297(2), Co2–P2 2.1159(20), Co1–C1 1.9520(8), Co1–C3 1.9520(8), Co2–C1 1.9520(8), Co2–C3 1.9741(8), Co1–C23 1.7949(10), Co1–C24 1.8096(10), Co2–C25 1.8032(10), Co2–C26 1.7996(93), C1–C3 1.3479(12), C1–C2 1.4893(12), C3–C4 1.4937(12), C2–O1 1.4101(13), C4–O2 1.4294(12), Co1–Co2–P2 174.500(9), Co2–Co1–P1 144.254(8), C23–Co1–C24 103.54(5), P1–Co1–C1 93.36(2), P1–Co1–C3 102.00(2), P2–Co2–C1 103.31(2), P2–Co2–C3 96.81(2).

investigation [35,36]. Structure–activity studies demonstrated that the activity depended strongly on the nature of the alkyne ligand so, the $\text{Co}_2(\text{CO})_6$ moiety has also been combined to several biomolecules such as carbohydrates (compound **E** in Chart 1 [37], nucleosides (compound **D** in Chart 1) [38,39] or peptides [40].

Even simple alkynes such as propargyl alcohol $\text{HC}\equiv\text{CCH}_2\text{OH}$, which is a non-bioactive molecule, give rise after coupling with $\text{Co}_2(\text{CO})_8$ to the hexacarbonyl derivative Co-Prop with an activity against MCF-7 cancer cells with IC₅₀ of 7.0 μM (compound **F** in Chart 1) [28]. Combination of the dicobalt carbonyl unit with a propargyl alcohol derivative should be a convenient way to allow secondary molecular interactions with biological targets via hydrogen bonding. Butynediol $\text{HOCH}_2\text{C}\equiv\text{CCH}_2\text{OH}$ (BUD) itself features only a limited biological activity [41], but the presence of two hydroxyl groups enhances its propensity to undergo extensive hydrogen bonding, which may be relevant for secondary interactions in an biological environment. Therefore BUD has been chosen for this study as an alkyne component since this unsaturated molecule is known to establish hydrogen bonding via its terminal OH groups, both in its organic solid state structure [42], in co-crystallisation with diverse ethene-1,2-diyl)dipyridines [43] or as π -ligand in organometallic coordination chemistry. Two examples are (η^2 -2-butyn-1,4-diol)-bis(triisopropylphosphine)nickel and (η^2 -but-2-yne-1,4-diol)-bis(triphenylphosphine)platinum [44,45]. In the crystal, the latter complex forms dimers, stabilized by hydrogen bonds between the hydroxy groups of adjacent molecules.

Furthermore, the internal alkyne BUD is readily bound to $[\text{Co}_2(\text{CO})_8]$, yielding an organometallic dimetallatetrahedrane cluster [24,46–48], whose framework can in turn, be modified by the so-called Nicholas reaction [49,50] or via substitution of CO by PR_3 , $\text{P}(\text{OR})_3$, and diphosphane ligands PR_2XPR_2 ($\text{X} = \text{CH}_2$, NH) [51–53]. Note that even heterodinuclear dimetallatetrahedrane frameworks with BUD, such as $[\text{Co}(\text{CO})_3(\mu\text{-HOCH}_2\text{C}\equiv\text{CCH}_2\text{OH})\text{CpMo}(\text{CO})_2]$ are literature-known [47]. Furthermore, there are some examples of polynuclear cobalt carbonyl clusters bearing BUD and featuring an interesting reactivity, such as dehydration of the activated alkyne [54]. BUD-functionalized silver nanoparticles have been probed recently for their antibacterial activity against *E. coli* [55]. The interaction of BUD within the nitrogenase MoFe protein has also been investigated [56].

Following our previous studies carried out on alkynol-based iron-platinum dimetallacyclopentenone complexes [57], the principal objective of this work was to synthesize a series of BUD-dicobalttetrahedrane complexes and to evaluate in a second step the anticancer activity of some derivatives through *in silico* simulation. With this objective in mind, we first present the synthesis of some novel dicobalt dimetallatetrahedranes and their exhaustive characterization by multinuclear NMR, X-ray diffraction, and Hirshfeld surfaces analyses. In the second part, after assessing their optimized electronic structures by DFT computing, we focused on the interaction of these cobalt homobimetallics in a biological environment with five target proteins: 2Q7K/2AX6 for prostate cancer, 1HK7/3EQM for breast cancer and 4FM9 for liver cancer. The degree of affinity between the target proteins and the homobimetallic scaffold was elucidated by means of *in silico* docking simulations.

2. Results and discussions

A series of dicobalt carbonyl compounds ligated by BUD was synthesized by modifying the phosphorus ligands ($\text{Ph}_2\text{PCH}_2\text{PPh}_2$, $\text{Ph}_2\text{PNRPPH}_2$ ($\text{R} = \text{H}$, Me), $\text{P}(\text{OAr})_3$ ($\text{Ar} = \text{Ph}$, Tol-*o*), and $\text{P}(\text{O}i\text{-Pr})_3$) to study the steric and electronic impact of the different framework architectures with respect to their interaction with the biological domain. All novel compounds were completely characterized in solution by IR and multinuclear NMR techniques, but a particular attention was devoted to the structural characterization at 100 K by single-crystal X-ray diffraction to analyze in addition to the molecular architectures their propensity to generate intra- and intermolecular secondary interactions.

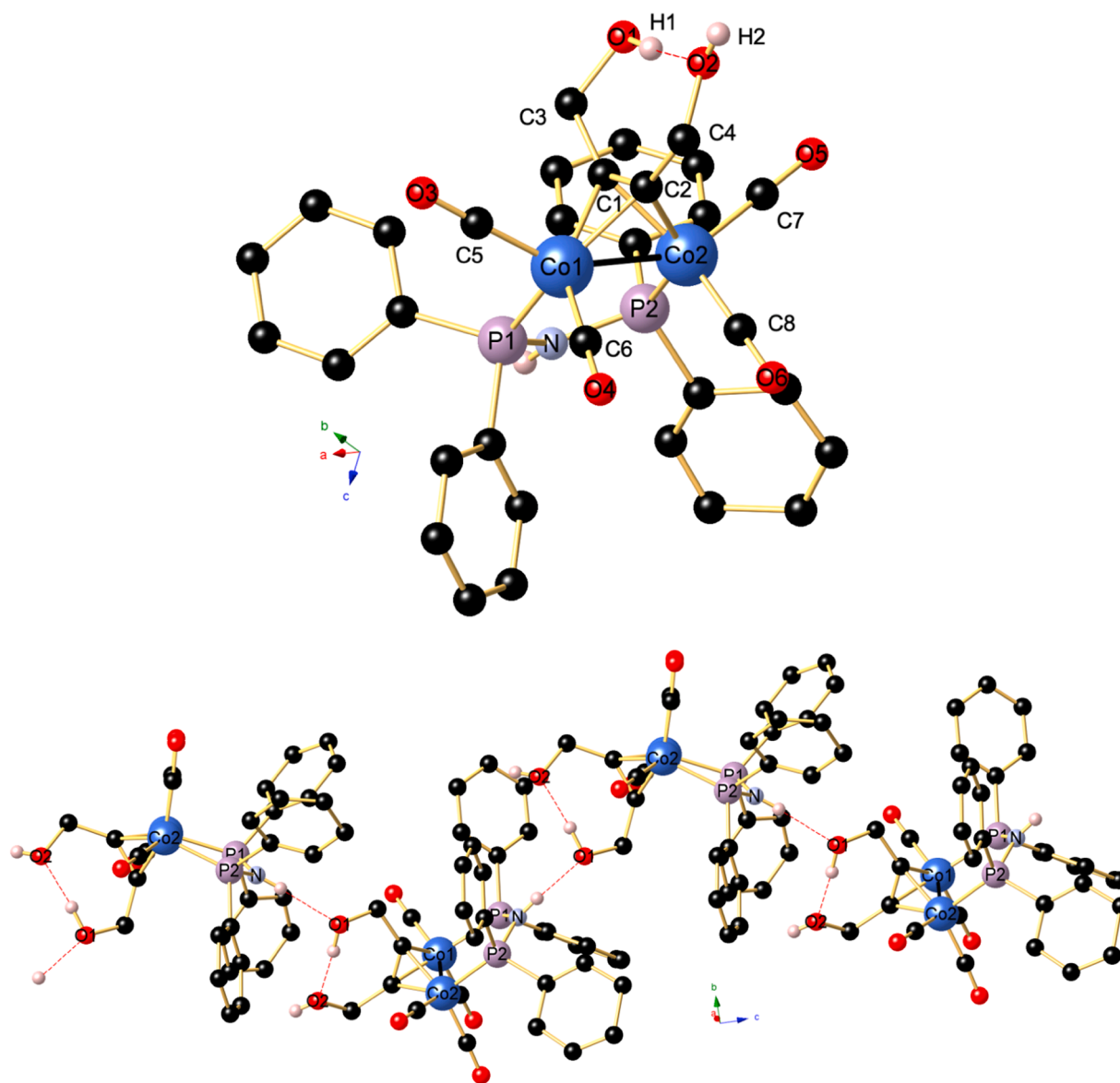


Fig. 3. (Top) Perspective view of **3a** showing the atom-labeling scheme. Hydrogen atoms apart from H1, H2, and N–H have been omitted for clarity. Selected distances (Å) and angles (°). Co1–Co2 2.4499(7), Co1–P1 2.2072(11), Co2–P2 2.2080(11), Co1–C1 1.962(4), Co1–C2 1.959(4), Co2–C1 1.9605(4), Co2–C2 1.943(4), Co1–C5 1.769(4), Co1–C6 1.797(4), Co2–C7 1.763(4), Co2–C8 1.768(5), C1–C2 1.353(5), C1–C3 1.486(5), C2–C4 1.487(5), C3–O1 1.431(4), C4–O2 1.426(5); Co1–Co2–P2 94.62(3), Co2–Co1–P1 97.52(3), Co1–C1–Co2 77.32(13), Co1–C2–Co2 77.79(14), C1–Co1–C2 40.37(14), P1–Co1–N1 113.20(12), P2–Co2–N2 111.25(12), P1–N1–P2 121.9(2). (Bottom) View of a segment of the supramolecular ribbon of **3a** running along the *c* axis, featuring both intra- and intermolecular O–H...O and N–H...O hydrogen bonding.

This supramolecular bonding may also be relevant for docking simulations in a biological environment.

This series of BUD-derived dimetallatetrahedranes, whose preparation is resumed in [Scheme 1](#), was completed by a series of structural-related complexes using thioether-functionalized alkynes $\text{RSCH}_2\text{C}\equiv\text{CCH}_2\text{SR}$ to investigate the effect of replacing OH by SR groups ([Scheme 2](#)).

2.1. Synthesis and crystal structure of $[\text{Co}_2(\text{CO})_6(\mu\text{-HOCH}_2\text{C}\equiv\text{CCH}_2\text{OH})]$ (**1**)

The synthesis of $[\text{Co}_2(\text{CO})_6(\mu\text{-HOCH}_2\text{C}\equiv\text{CCH}_2\text{OH})]$ (**1**), obtained by treatment of $[\text{Co}_2(\text{CO})_8]$ with BUD ([Scheme 1](#)) was first described by Wotiz *et al.* in 1954 [24]. This air-stable red crystalline compound has also been crystallographically characterized at 295 K as monohydrate (space group $P2_1/c$, CSD ref code BIPGOW10) by Coppens *et al.*, in 1984

[46] and its dimetallatetrahedrane framework established. A second structural characterization was performed in 1998 by Gruselle *et al.*, (space group $C2/c$, CSD ref code JOZWUQ) [47]. Based on the O...O separation ($d(\text{O1}–\text{O2})$ 2.754 Å) and angles between the two hydroxyl groups, the authors suggested the occurrence of an intramolecular hydrogen bonding. To obtain a better-resolved structure, we redetermined the crystal structure of **1** at 100 K. Although we failed to refine all H positions, the quality of the data set allows a more accurate discussion of the hydrogen bonding. Like structure JOZWUQ, our product **1** crystallized in the monoclinic space group $C2/c$ (Table S1). [Fig. 1](#) (top) shows the molecular structure of the dicobaltatetrahedrane framework, in which the two crystallographically non-equivalent cobalt centers are linked by a metal–metal bond of 2.4750(6) Å. A detailed structural discussion is unnecessary since the metric parameters are very similar to those reported for the 295 K structure JOZWUQ. [Fig. 1](#) (bottom) shows that H1 attached on O1 interacts with the hydroxyl group of O2 forming

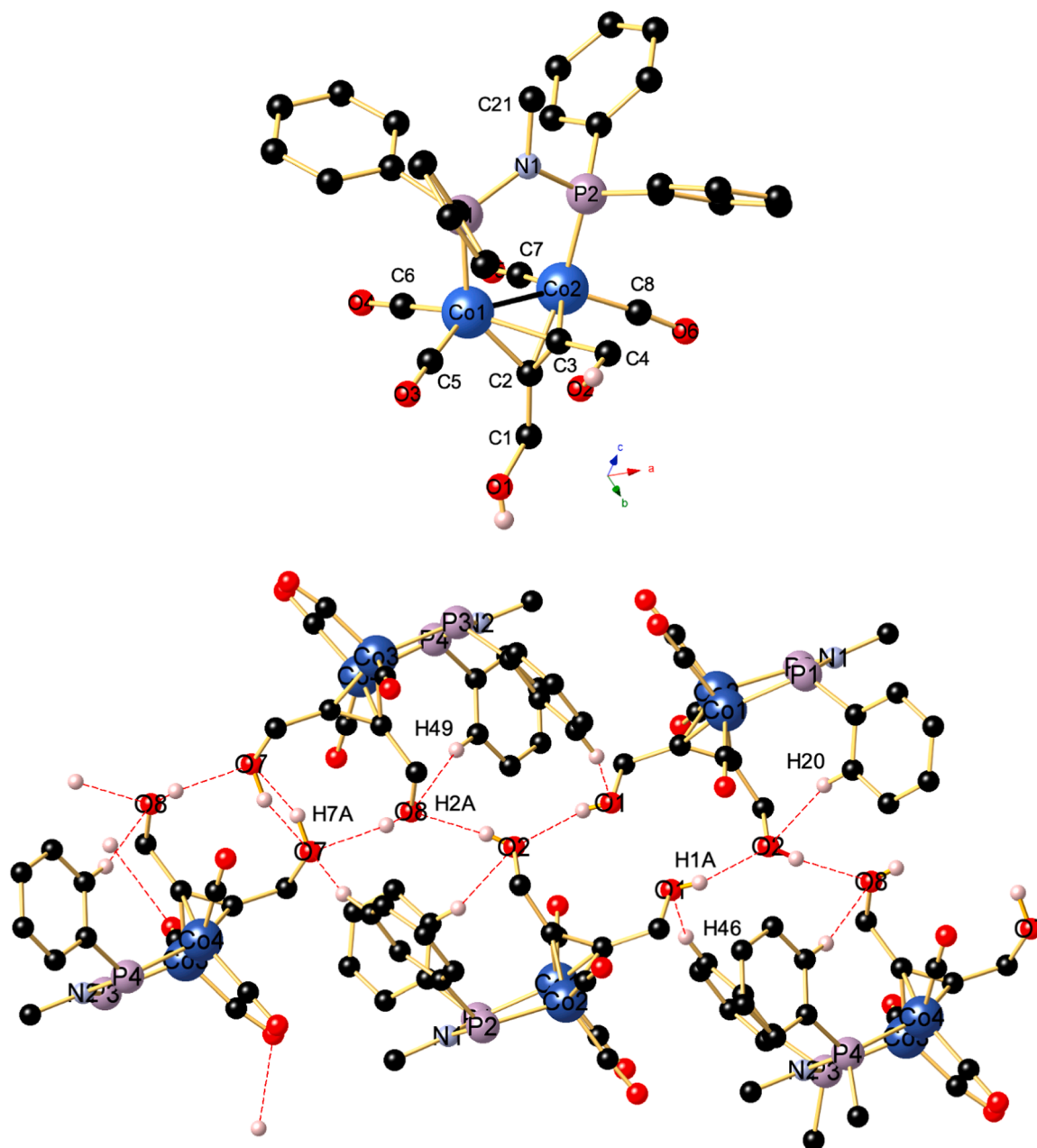


Fig. 4. (top) Perspective view of **3b** showing the atom-labeling scheme. Only molecule M1 of the two independent molecules is shown. Hydrogen atoms apart from H1 and H2 have been omitted for clarity. Selected distances (Å) and angles ($^{\circ}$). Co1–Co2 2.4389(5), Co1–P1 2.1958(7), Co2–P2 2.1918(7), Co1–C2 1.935(2), Co1–C3 1.960(24), Co2–C2 1.946(2), Co2–C3 1.959(2), Co1–C5 1.771(2), Co1–C6 1.791(2), Co2–C7 1.782(2), Co2–C8 1.764(25), C1–C2 1.480(3), C2–C3 1.342(3), C3–C4 1.491(3), C1–O1 1.426(3), C4–O2 1.427(5); Co1–Co2–P2 96.26(2), Co2–Co1–P1 95.94(2), Co1–C2–Co2 77.88(8), Co1–C3–Co2 76.98(8), C1–Co1–C2 40.37(14), Co1–P1–N1 113.59(7), Co2–P2–N1 113.47(7), P1–N1–P2 119.43(11). (Bottom) View of a segment of the supramolecular network of **3b**, featuring both intra- and intermolecular C–H...O and O–H...O hydrogen bonding. Some phenyl groups have been omitted for clarity. Symmetry operations used to generate equivalent atoms: $^{\#}1-x, 1-y, 1-z$; $^{\#}2-x, 2-y, 1-z$.

an intramolecular seven-membered cycle with $d(\text{O1}–\text{H1}\cdots\text{O2}) = 1.89 \text{ \AA}$, $d(\text{O1}–\text{O2}) = 2.725(3) \text{ \AA}$ and an angle $\text{O1}–\text{H1}\cdots\text{O2}$ of 171.6° . A second intermolecular hydrogen bonding occurs between the $\text{O2}–\text{H2}$ hydroxyl groups of two adjacent molecules forming a supramolecular dimer with $d(\text{O2}–\text{H2}\cdots\text{O2}') = 1.93 \text{ \AA}$ and an angle $\text{O2}–\text{H2}\cdots\text{O2}'$ of 152.7° . Note that the positions of H1 and H2 could not be refined freely and are calculated, but taking in account the $\text{O}\cdots\text{O}$ separations, the above discussion about $\text{O}–\text{H}\cdots\text{O}$ contacts seems sufficiently accurate. Apart from a weak intermolecular contact of 2.987 \AA between the O6 and O7 $^{\#}$ atoms of two carbonyl groups, no other contacts were identified (symmetry code $^{\#}1.5-x, -1/2+y, 1.5-z$).

2.2. Synthesis and crystal structure of $[\text{Co}_2(\text{CO})_4\{\text{P}(\text{O}^i\text{Ph})_3\}_2(\mu\text{-HOCH}_2\text{C}\equiv\text{CCH}_2\text{OH})]$ (**2a**)

We have recently shown that $[\text{Co}_2(\text{CO})_6\{\text{P}(\text{O}^i\text{Ph})_3\}_2]$ is a suitable starting material for triphenylphosphite-substituted complexes $[\text{Co}_2(\text{CO})_4\{\text{P}(\text{O}^i\text{Ph})_3\}_2(\mu\text{-RC}\equiv\text{CR})]$ ($\text{R} = \text{H}, \text{Ph}$) [58]. To evaluate the impact of the replacement of carbonyl by the stronger donor $\text{P}(\text{O}^i\text{Ph})_3$ on the structural characteristics and hydrogen bonding of the dimetallate-tetrahedrane framework, we reacted $[\text{Co}_2(\text{CO})_6\{\text{P}(\text{O}^i\text{Ph})_3\}_2]$ with BUD according to Scheme 1 in hot toluene. The targeted compound $[\text{Co}_2(\text{CO})_4\{\text{P}(\text{O}^i\text{Ph})_3\}_2(\mu\text{-HOCH}_2\text{C}\equiv\text{CCH}_2\text{OH})]$ (**2a**) was isolated in the form of red air-stable crystals. The presence of $\text{P}(\text{O}^i\text{Ph})_3$ is indicated by a

broad singlet resonance in the $^{31}\text{P}\{^1\text{H}\}$ NMR at δ 152.3 ppm and a decrease in the CO-stretching frequencies is induced as a result of a stronger electron density on the metal centers (Table 1). A well resolved ^1H NMR spectrum was obtained in CDCl_3 and the signal for the hydroxyl protons appears as a triplet centered at δ 2.22 ppm ($^3J_{\text{HH}} = 6.1$ Hz), due to coupling with the $-\text{OCH}_2-$ group, which is observed as a doublet at δ 4.80 ppm ($^3J_{\text{HH}} = 6.1$ Hz). The ^{13}C NMR spectrum exhibits 7 peaks with resonances corresponding to the BUD moiety at δ 91.8 and 63.6 ppm, assigned the tetrahedrane carbons and CH_2O , respectively. The four

carbonyls give rise to just one singlet at δ 203.3 ppm without resolved PC coupling (Figs. S1-S3).

Fig. 2 shows the molecular structure of **2a** in which the BUD moiety is almost orthogonally arranged with respect to the Co–Co vector ($91.53(5)^\circ$) (Table S1). The two crystallographically non-equivalent $\text{P}(\text{O}^i\text{Ph})_3$ ligands have lost their ideal linear *trans*-disposition of 180° occurring in precursor $[\text{Co}_2(\text{CO})_6\{\text{P}(\text{O}^i\text{Ph})_3\}_2]$, the dihedral angle P1–Co1–Co2–P2 being now $43.82(5)^\circ$. Note that for $[\text{Co}_2(\text{CO})_4\{\text{P}(\text{O}^i\text{Ph})_3\}_2(\mu\text{-H}\equiv\text{CCH}_2\text{Ph})]$ this dihedral angle is much more flattened with 11.96° .

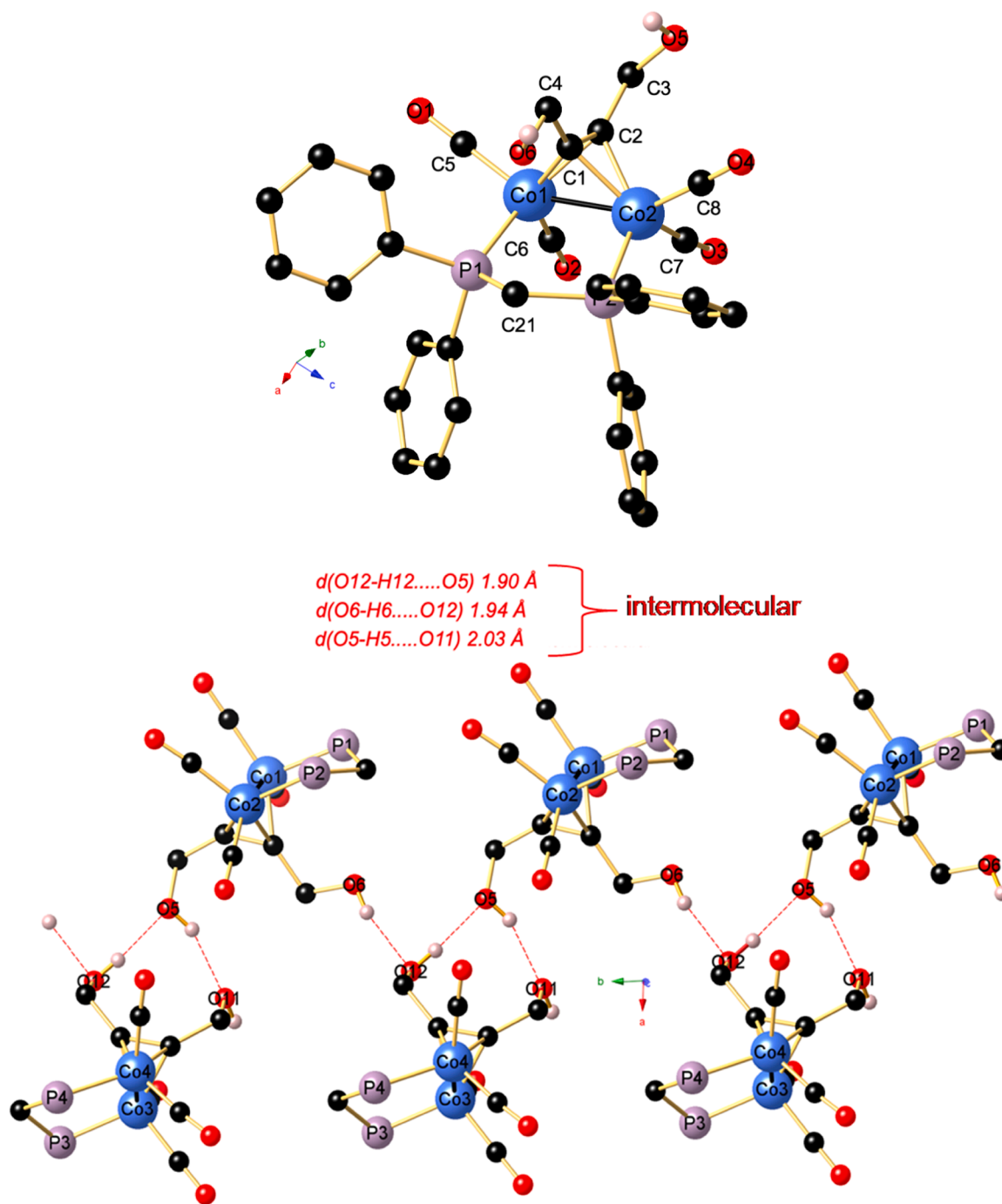


Fig. 5. (Top) Perspective view of **3c** showing the atom-labeling scheme. Only molecule **M1** of the two independent molecules is shown. Hydrogen atoms apart from H5, H6 and H12 have been omitted for clarity. Selected distances (Å) and angles ($^\circ$). Co1–Co2 2.4752(11), Co1–P1 2.2182(15), Co2–P2 2.2257(14), Co1–C1 1.966(4), Co1–C2 1.948(2), Co2–C1 1.964(4), Co2–C2 1.961(4), Co1–C5 1.7979(4), Co1–C6 1.794(4), Co2–C7 1.786(5), Co2–C8 1.773(5), C1–C2 1.346(64), C1–C4 1.500(6), C2–C43 1.476(6), C3–O5 1.451(5), C4–O6 1.414(6); Co1–Co2–P2 95.91(4), Co2–Co1–P1 98.03(4), Co1–C1–Co2 78.06(16), Co1–C2–Co2 78.59(16), C1–Co1–C2 40.24(18), P1–Co1–C5 98.67(15), P1–Co1–C6 102.25(15), P2–Co2–C7 112.15(15), P2–Co2–C8 97.95(17). (Bottom) View of a segment of the supramolecular ribbon of **3c** running along the *b* axis, featuring intermolecular O–H \cdots O hydrogen bonding. The phenyl groups have been omitted for clarity.

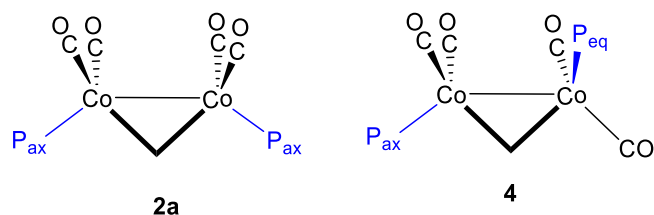


Fig. 6. Axial or equatorial positions and relative orientation of the $P(OPh)_3$ ligands in compounds **2a** and **4**. The acetylenic substituents have been omitted for clarity.

The mean Co–P distance of **2a** differs not much from that of its phenylacetylene analogue (2.1228(2) vs. 2.1303(7) Å). The Co–Co bond length is shortened with respect to that of **1** (2.4588(17) vs. 2.4750(6) Å) and that of $[Co_2(CO)_4\{P(OPh)_3\}_2(\mu-HC\equiv CCH_2Ph)]$ (2.4666(5) Å). Surprisingly, no intermolecular O–H...O bonding could be detected for **2a** using the MERCURY software. Only a weak intramolecular O2–H2...O interaction of 2.249(19) Å with the O11 atom of a $P(OPh)_3$ ligand could be evidenced, giving rise to a seven-membered ring with an angle O2–H2...O11 of 158.0(17)°. Furthermore, O12 of a $P(OPh)_3$ ligand interacts with the *o*-H atom of a phenyl cycle with $d(H32...O12)$ 2.530(16) Å.

2.3. Synthesis of $[Co_2(CO)_4\{P(OTol-o)_3\}_2(\mu-HOCH_2C\equiv CCH_2OH)]$ (**2b**) and $[Co_2(CO)_4\{P(OPr-i)_3\}_2(\mu-HOCH_2C\equiv CCH_2OH)]$ (**2c**)

We have recently reported on the crystal structure of $[Co_2(CO)_6\{P(OTol-o)_3\}_2]$ and the reaction of this dinuclear complex with diphenylacetylene yielding crystallographically characterized $[(o-TolO)_3P(OC)_2Co-Co(\mu-PhC\equiv CPh)(CO)_2\{P(OTol-o)_3\}]$, in which the two sterically crowded tri-*o*-tolylphosphite ligands adopt a similar arrangement as found for **2a**, with a dihedral angle P–Co–Co–P of 5.50(7)° [58]. Note that the Tolman cone angle Θ is used as descriptor of the steric measure of PR_3 ligand. The cone angle of $P(OPh)_3$ is reported to be 128°, whereas that of $P(OTol-o)_3$ is 141° [59,60]. To evaluate the steric effect on the structure, we reacted also $[Co_2(CO)_6\{P(OTol-o)_3\}_2]$ with BUD (Scheme 1) and isolated **2b** as a red solid. Unfortunately, we failed to obtain X-ray-suitable crystals of **2b**. However, the similarity of the IR spectra of **2a** and **2b** strongly suggests that the geometries of both complexes are quite close. The 1H NMR spectra shows a line-broadening of all peaks, probably due to the quadrupolar relaxation of the ^{59}Co -nuclei [61,62].

To investigate the impact of an enhanced electron-density of the bimetallic framework on the molecular geometry and hydrogen bonding, we prepared $[Co_2(CO)_6\{P(OPr-i)_3\}_2]$ [63] bearing two

triisopropylphosphite ligands as precursor and reacted it with BUD in toluene (Scheme 1). Note that $P(OPr-i)_3$ is a stronger electron-donor ligand compared to $P(OPh)_3$, but their cone angle Θ are quite comparable (130° vs. 128°) [59,60]. The targeted compound $[Co_2(CO)_4\{P(OPr-i)_3\}_2(\mu-HOCH_2C\equiv CCH_2OH)]$ (**2c**) was formed in high yield but was isolated as a red waxy solid, excluding any crystallographic characterization. Alternatively, we prepared **2c** by CO substitution of **1** by adding two equivalents of $P(OPr-i)_3$, but again, the purified product **2c** had a waxy consistency. However, the IR and NMR data clearly corroborate the formation of **2c**. In the ^{31}P NMR spectrum, a broad singlet at 157.4 ppm is attributed to the $P(OPr-i)_3$ ligand. The IR(ATR) spectrum in the 1900–2100 cm^{-1} zone shows two strong carbonyl absorptions at 2021 (s) and 1960 (vs, br) cm^{-1} consistent with the stronger electron-donor propensity of $P(OPr-i)_3$ compared to $P(OPh)_3$. These data are similar to those of the other phosphite complexes **2a** and **2b** (**2a**: δ_P 152.3 ppm and 2046 (s), 2000 (s), 1984(vs), 1969(s) cm^{-1} ; **2b**: δ_P 148.5 ppm and 2040 (s), 2003 (s), 1982 (vs) cm^{-1}). In CH_2Cl_2 solution, only two terminal carbonyl stretching vibrations were observed for **2a-c**, the one at the lower wavenumber being broad. The ^{13}C NMR of **2c** displays at 205.9 and 88.5 ppm resonances due to the carbonyl groups and the acetylenic moiety coordinated to the cobalt atoms. Three resonances between 23–73 ppm are assigned to the aliphatic carbons. Three further signals in this range and an additional singlet at -3.4 ppm in the ^{31}P NMR spectrum could be attributed to the presence of the phosphite oxide $O=P(OPr-i)_3$ as an impurity. We suggest that the two $P(OPr-i)_3$ ligands of **2c** occupy a pseudo-axial coordination site of the dinuclear framework as encountered for **2a** (see also Fig. 6). Such an axial arrangement has also been evidenced for the tetranuclear diyne-bridged compound $(\mu_4-\eta^2, \eta^2-1,5-bis(2-(phenyl)ethynyl)naphthalene)-octacarbonyl-tetrakis(trimethoxyphosphite)-tetracobalt$ (CSD refcode DAPQEQ), where the two $P(OMe)_3$ ligands of each P–Co–Co–P moiety adopt a torsion angle of 3.51° [64].

2.4. Synthesis and crystal structure of $[Co_2(CO)_4(\mu-dppa)(\mu-HOCH_2C\equiv CCH_2OH)]$ (**3a**) and $[Co_2(CO)_4(\mu-Medppa)(\mu-HOCH_2C\equiv CCH_2OH)]$ (**3b**)

The use of diphosphane ligands of the type Ar_2PXPAr_2 as molecular clamps is a common tool in dicobaltatetrahydride chemistry to shorten and stabilize the metal-metal bond and force a particular architecture involving a rigid five-membered Co–P–X–P–Co cycle [53]. In addition to these structural and stability aspects, the potential of μ -diphosphane bridged bimetallic complexes is emerging in anticancer research, as witnessed by a recent review article [65]. There are numerous articles describing the assembly of these scaffolds by *i*) addition of Ar_2PXPAr_2 to

Table 2

Selected experimental and calculated bond lengths (Å) and angles (°) (C_t = tetrahedrane carbon atoms, C_{eq} = C pseudo-equatorial, C_{ax} = C pseudo-axial)

		Co–Co	C_t – C_t	Co– C_t	Co– C_{eq}	Co– C_{ax}	Co–P	C_t – C_t – CH_2	Co–Co–P
1	Exp.	2.475	1.325	1.963	1.825	1.805		137.6	-
	Calc.	2.473	1.350	1.953	1.825	1.778		135.3	-
2a	Exp.	2.459	1.348	1.958	1.802	-	2.123	140.1	145.877
	Calc.	2.439	1.359	1.993	1.781	-	2.321	137.8	113.461
2c	Exp.	2.406	1.337	1.960	1.783	-	2.271	121.2	106.5
	Calc.								145.6
3a	Exp.	2.450	1.353	1.956	1.782	1.766	2.208	137.4	96.1
	Calc.	2.453	1.350	1.946	1.791	1.763	2.306	139.3	96.3
3b	Exp.	2.439	1.342	1.950	1.787	1.768	2.194	141.6	96.1
	Calc.	2.475	1.346	1.960	1.790	1.776	2.222	137.5	97.0
3c	Exp.	2.458	1.357	1.938	1.790	1.769	2.321	135.3	97.5
	Calc.	2.480	1.323	1.962	1.804	1.784	2.123	138.2	102.8
4	Exp.						2.164		147.6
	Calc.	2.434	1.339	1.952	1.784	1.775	2.268	137.4	105.4
5a	Exp.	2.459	1.343	1.954	1.799	1.781	2.199	140.3	95.9
	Calc.	2.552	1.444	1.850	1.784	1.769	2.279	141.1	97.8
5b	Exp.	2.452	1.346	1.959	1.794	1.769	2.202	140.8	96.6
	Calc.	2.458	1.367	1.984	1.778	1.776	2.332	141.0	97.7

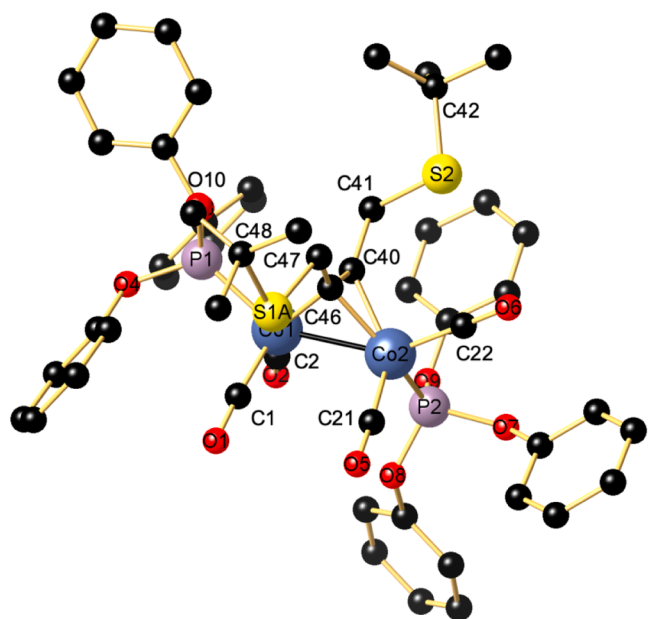


Fig. 7. Perspective view of **4** showing the atom-labeling scheme. Hydrogen atoms have been omitted for clarity. Selected distances (Å) and angles (°). Co1–Co2 2.47975(19), Co1–P1 2.12310(15), Co2–P2 2.1643(20), Co1–C1 1.8081(4), Co1–C2 1.7954(3), Co2–C21 1.8084(4), Co2–C22 1.7837(4), Co1–C40 1.9622(3), Co1–C46 1.9650(3), Co2–C40 1.9663(3), Co2–C46 1.9535(3), C40–C46 1.3227(4), C40–C41 1.4892(5), C46–C47 1.4899(4), C47–S1A 1.8123(8), C41–S2 1.8223(4); Co1–Co2–P2 102.788(5), Co2–Co1–P1 147.583(5), C1–Co1–C2 102.723(16), P1–Co1–C40 99.241(11), P1–Co1–C46 99.474(11), P2–Co2–C40 111.213(10), P2–Co2–C46 148.286(10).

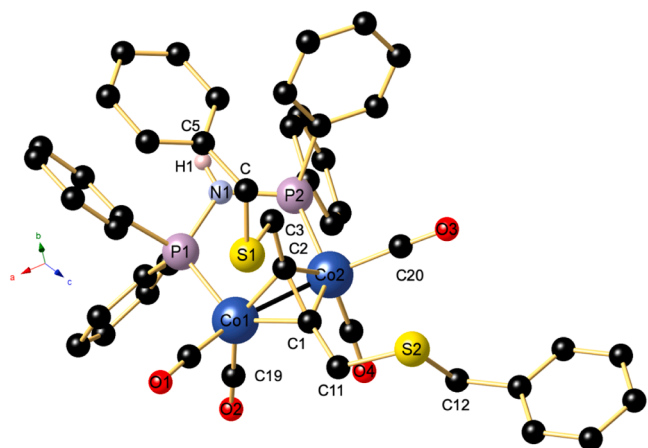


Fig. 8. Perspective view of **5b** showing the atom-labeling scheme. Apart of H1, all hydrogen atoms have been omitted for clarity. Only molecule 1 of the two independent molecules present in the asymmetric unit is shown. Selected distances (Å) and angles (°). Co1–Co2 2.4520(8), Co1–P1 2.2043(9), Co2–P2 2.2007(10), Co1–C1 1.9598(17), Co1–C2 1.9612(17), Co2–C1 1.9510(17), Co2–C2 1.9653(16), C1–C2 1.346(2), C1–C11 1.486(2), C1–S2 1.8228(18), C2–C3 1.487(2), C3–S1 1.8250(12), P1–N1 1.6960(14), P2–N1 1.6917(15); Co1–Co2–P2 97.752(6), Co2–Co1–P1 95.67(3), Co1–C1–Co2 77.65(6), Co1–C2–Co2 77.26(6), P1–Co1–Co2 95.67(3), P2–Co2–Co1 97.51(3), Co1–P1–N1 112.05(6), Co2–P2–N1 110.95(5), P1–N1–P2 118.68(18).

an existing dicobalttetrahedrane compound or ii) reaction of a $[\text{Co}_2(\text{CO})_6(\mu\text{-Ar}_2\text{PXPAr}_2)]$ with a given alkyne. In the case of bis(diphenylphosphino)amine $\text{Ph}_2\text{PNHPPH}_2$ (dppa), the group of Ellermann has described in 1996 the preparation of $[\text{Co}_2(\text{CO})_4(\mu\text{-dppa})(\mu\text{-HOCH}_2\text{C}\equiv\text{CCH}_2\text{OH})]$ (**3a**) via carbonyl substitution of $[\text{Co}_2(\mu_2\text{-CO})_2(\text{CO})_4(\mu\text{-dppa})]$ by BUD in THF as solvent [66]. The

resulting complex was isolated in the form of deep-red crystalline material and characterized thoroughly by multinuclear NMR and IR studies, indicating the occurrence of $\text{N}\cdots\text{H}\cdots\text{O}$ hydrogen bonding with a THF molecule. However, this group failed to obtain X-ray suitable single crystals. We repeated this synthesis by employing warm toluene instead of THF (Scheme 1) and growing single crystals crystallizing in the monoclinic space group $C2/c$ (Table S2). The molecular structure of **3a** determined at 100 K is illustrated in Fig. 3 and shows two crystallographically different Co centers, which are linked by metal-metal bond. Compared to unsupported **1**, that of **3a** is shortened (2.4750(6) vs. 2.4499(7) Å) and may be compared with those of $[\text{Co}_2(\text{CO})_4(\mu\text{-dppa})(\mu\text{-HC}\equiv\text{CCH}_2\text{OH})]$ (2.4675(7) Å) [67] and $[\text{Co}_2(\text{CO})_4(\mu\text{-dppa})(\mu\text{-HC}\equiv\text{C-PCP})]$ (PCP = [2.2]-paracyclophane (2.4627(5) Å) [68]. The spanning dppa ligand, whose two P atoms are perpendicular with respect to the Co–Co vector, forms a five-membered cycle with an envelope conformation. The BUD unit is orthogonally arranged as in **1** and **2a**. In a very meticulous IR study performed on $[\text{Co}_2(\text{CO})_4(\mu\text{-dppa})(\mu\text{-OHCH}_2\text{C}\equiv\text{CCH}_2\text{OH})] \times \text{THF}$, the authors attribute a band at 1578 cm^{-1} to the $\nu(\text{C}=\text{C})$ vibration of the two central carbon atoms of the π -coordinated alkyne (for free BUD at 2212 cm^{-1}). This allows to estimate the bond order to be about 1.8 [64]. For **3a**, the bond length between C1–C2 is $1.353(5)\text{ Å}$, close to the average value of the C=C bond of alkenes (1.34 Å), but shorter than that of π -coordinated *cis*-1,4-butadiene in the salt $\text{PPh}_4[\text{PtCl}_3(\mu\text{-HOCH}_2\text{C}\equiv\text{CCH}_2\text{OH})]$ ($1.40(4)\text{ Å}$) [69].

In line with the IR data reported by Ellermann, the observation of several broadened bands in the range between $3200\text{--}3600\text{ cm}^{-1}$ (Fig. S4) indicates the occurrence of $\text{O}\cdots\text{H}\cdots\text{O}$ bonding. Indeed, in **3a** the H1 atom attached to O1 interacts with O2 ($d(\text{O1}\cdots\text{H1}\cdots\text{O2})\ 1.80(6)\text{ Å}$; $d(\text{O1}\cdots\text{O2})\ 2.763(4)\text{ Å}$) of the second hydroxyl group, forming a seven-membered cycle with an angle ($\text{O1}\cdots\text{H1}\cdots\text{O2}$) of $176(5)^\circ$. In contrast, the hydroxyl group O2H2 does not participate in any bonding. The molecular cell with $Z = 8$ contains 4 pairwise arranged **3a** molecules (Table S2). Fig. 3 (bottom) shows that in the crystal, the individual molecules are furthermore interconnected through hydrogen bridges formed between the N–H group of dppa and the O1 atom of a neighbored molecule with $d(\text{N}\cdots\text{H1A}\cdots\text{O1}^1)\ 2.10(4)\text{ Å}$, generating a 1D supramolecular ribbon. Similar 1D intermolecular arrangement based on $\text{N}\cdots\text{H}\cdots\text{OH}$ hydrogen bonding is encountered in other crystallographically characterized $[\text{Co}_2(\text{CO})_4(\mu\text{-dppa})(\mu\text{-alkynol})]$ compounds such as $[\text{Co}_2(\text{CO})_4(\mu\text{-dppa})(\mu\text{-HC}\equiv\text{CPh}_2\text{OH})]$ ($d(\text{NH}\cdots\text{O})\ 2.231\text{ Å}$, $d(\text{N}\cdots\text{O})\ 3.052\text{ Å}$, angle $\text{NHO}\ 159^\circ$), $[\text{Co}_2(\text{CO})_4(\mu\text{-dppa})(\mu\text{-HC}\equiv\text{CCH}_2\text{OH})]$ ($d(\text{NH}\cdots\text{O})\ 2.116\text{ Å}$, $d(\text{N}\cdots\text{O})\ 2.888\text{ Å}$, angle $\text{NHO}\ 173^\circ$; $d(\text{NH}\cdots\text{O})\ 2.125\text{ Å}$, $d(\text{NO})\ 2.909\text{ Å}$, angle $\text{NHO}\ 177^\circ$) and $[\text{Co}_2(\text{CO})_4(\mu\text{-dppa})(\mu\text{-HC}\equiv\text{C}(\text{CH}_2)_2\text{OH})]$ ($d(\text{NH}\cdots\text{O})\ 2.104\text{ Å}$, $d(\text{N}\cdots\text{O})\ 2.961\text{ Å}$, angle $\text{NHO}\ 175^\circ$; $d(\text{NH}\cdots\text{O})\ 2.126\text{ Å}$, $d(\text{NO})\ 2.963\text{ Å}$, angle $\text{NHO}\ 164^\circ$) [64].

By treatment of *in situ* prepared $[\text{Co}_2(\mu_2\text{-CO})_2(\text{CO})_4(\mu\text{-Medppa})]$ (yet unknown in the literature) with BUD in warm toluene, we succeeded also to synthesize $[\text{Co}_2(\text{CO})_4(\mu\text{-Medppa})(\mu\text{-HOCH}_2\text{C}\equiv\text{CCH}_2\text{OH})]$ (**3b**). In the IR(ATR) spectrum, four carbonyl frequencies are present at 2018, 1988, 1963, and 1942 cm^{-1} and in the ^{31}P NMR spectrum, a broad singlet is observed at 115.1 ppm. The resonance due to the NMe group appears at 35.0 ppm in the ^{13}C NMR, and in the ^1H NMR spectrum the $^3J_{\text{PH}}$ coupling with the two chemically equivalent P-atoms gives rise to a broad triplet with a coupling constant of 4.8 Hz. Crystals of this red compound were grown from toluene layered with heptane. The asymmetric unit contains two independent molecules. Fig. 4 (top) shows molecule **M1**, which has, among all BUD complexes **1–3d**, the shortest Co–Co bond length ($2.4389(5)\text{ Å}$). In molecule **M2**, the intermetallic distance is $2.4505(5)\text{ Å}$. There is just one other example of a Medppa-bridged dicobalttetrahedrane in the literature, namely $[\text{Co}_2(\text{CO})_4(\mu\text{-Medppa})(\mu\text{-HC}\equiv\text{CPh})]$ with $d(\text{Co}\cdots\text{Co})$ of $2.44451(4)\text{ Å}$ [53]. Contrary to its dppa counterpart **3a**, the two hydroxyl groups of **3c** are with $d(\text{O}\cdots\text{O})\ 4.103\text{ Å}$ quite remote, excluding any intramolecular $\text{O}\cdots\text{H}\cdots\text{O}$ hydrogen bonding. The hydroxyl protons showed a crystallographic disorder (part A/part B) that fortunately could be resolved. For clarity, only the A part

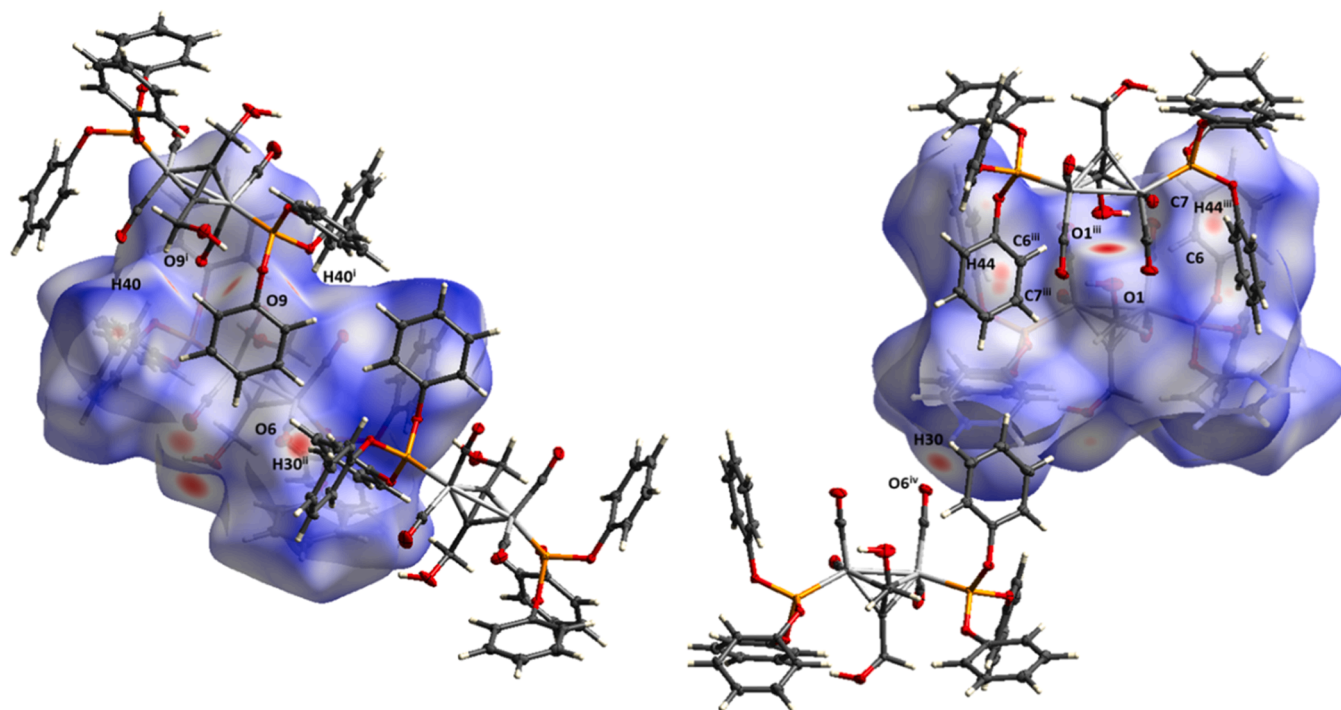


Fig. 9. Hirshfeld surface of compound 2a mapped with d_{norm} over the range $-0.2219 - 1.4979$ a.u. Symmetry codes: i = $-x+1, -y+1, -z+1$; ii = $-x-1, y+1, +z$; iii = $-x+1, -y+2, -z+2$, and iv = $x+1, y-1, +z$.

will be discussed in the following. In contrast, an extensive intermolecular hydrogen bonding ranging from 1.72(5) to 2.02(07) Å occurs between the O7–H7A groups of two adjacent independent molecules 1 and 2, between O1–H1A and O2 (1.95(6) Å), between O2–H2A and O8 (1.97(6) Å) as well between O8–H8A and O7 (Fig. 4 bottom). Furthermore, several aromatic C–H...O contacts exist between C20–H20...O2, C46–H46...O1, and C49–H49...O8.

2.5. Synthesis and crystal structure of $[\text{Co}_2(\text{CO})_4(\mu\text{-dppm})(\mu\text{-HOCH}_2\text{C}\equiv\text{CCH}_2\text{OH})]$ (3c)

This series of diphosphane-spanned derivatives has been completed by the synthesis of $[\text{Co}_2(\text{CO})_4(\mu\text{-dppm})(\mu\text{-HOCH}_2\text{C}\equiv\text{CCH}_2\text{OH})]$ (3c), obtained by reaction of $[\text{Co}_2(\text{CO})_6(\mu\text{-Ph}_2\text{PCH}_2\text{PPh}_2)]$ with BUD in toluene (Scheme 1). The IR spectrum in the $\nu(\text{CO})$ region and the NMR data are similar to those of other dppm-bridged Co–Co complexes such as $[\text{Co}_2(\text{CO})_4(\mu\text{-dppm})(\mu\text{-HOCPh}_2\text{C}\equiv\text{CCPh}_2\text{OH})]$ [67] and deserve no particular comment (Table 1). Compound 3c crystallizes in the monoclinic crystal system, space group $C2/c$ and the asymmetric unit contains two independent molecules M1 and M2 (Table S2). One is presented in

Fig. 5, showing the tetrahedrane Co_2C_2 arrangement (see caption of Fig. 5). The dppm ligand occupies two equatorial positions, as already observed in other dppm-bridged dicobaltatetrahedrane complexes [64, 67]. The relative orientation of the hydroxyl groups of the BUD unit prevents the formation of intramolecular hydrogen bonds but the two crystallographically independent molecules pack by such intermolecular interactions involving each OH with $d(\text{O5H5}\cdots\text{O11}^1)$ 2.03 Å, $d(\text{O5}\cdots\text{O11}^1)$ 2.768(5) Å, angle O5-H5-O11^1 145.8° (symmetry code $^1+x, 1+y, +z$), $d(\text{O12H12A}\cdots\text{O5}^2)$ 1.90 Å, $d(\text{O12}\cdots\text{O5}^2)$ 2.727(5) Å, angle O12-H12A-O5^2 169.6° (symmetry code $^2+x, -1+y, +z$) and $d(\text{O6H6}\cdots\text{O12})$ 1.94 Å, $d(\text{O6}\cdots\text{O12})$ 2.748(5) Å, angle O6-H6-O12 162.5°.

2.6. Synthesis and crystal structure of $[\text{Co}_2(\text{CO})_4\{\text{P}(\text{O}^i\text{Ph})_3\}_2(\mu\text{-}t\text{-BuSCH}_2\text{C}\equiv\text{CCH}_2\text{S}^i\text{Bu-}t)]$ (4)

Thioethers R-S-R play also an important in biology and are for example present in some amino acids such as methionine (<https://en.wikipedia.org/wiki/Methionine>). This motivated us to extend our investigation on $[\text{Co}_2(\text{CO})_4\text{L}_2(\mu\text{-RSCH}_2\text{C}\equiv\text{CCH}_2\text{SR})]$ complexes, in which the OH hydroxyl groups are replaced by -SR thioether functions. In the so-called Nicholas reaction [49,50,70] a dicobalt hexacarbonyl-stabilized propargylic cation $[\text{Co}_2(\text{CO})_6(\mu\text{-R}_1\text{C}\equiv\text{C-CR}_2\text{R}_3)]^+$, generated by treatment of $[\text{Co}_2(\text{CO})_8]$ with a propargylic ether $\text{R}_1\text{C}\equiv\text{C-C}(\text{OR})\text{R}_2\text{R}_3$ or an alkynol $\text{R}_1\text{C}\equiv\text{C-C}(\text{OH})\text{R}_2\text{R}_3$ and subsequent treatment with a Lewis acid, is reacted with a nucleophile (Nuc) leading to $[\text{Co}_2(\text{CO})_6(\mu\text{-R}_1\text{C}\equiv\text{C-C}(\text{Nuc})\text{R}_2\text{R}_3)]$.

Went and coworkers have applied this generation of dicobalt hexacarbonyl-stabilized propargylic cation in a series of papers to convert $[\text{Co}_2(\text{CO})_6(\mu\text{-HOCH}_2\text{C}\equiv\text{CCH}_2\text{OH})]$ (1) to thioether-functionalized species $[\text{Co}_2(\text{CO})_6(\mu\text{-RSCH}_2\text{C}\equiv\text{CCH}_2\text{SR})]$ by treatment of 1 with thiols RSH in the presence of Lewis acids such as HBF_4 [71,72]. For example, the reaction of 1 with $t\text{-BuSH}$ is reported to afford $[\text{Co}_2(\text{CO})_6(\mu\text{-}t\text{-BuSCH}_2\text{C}\equiv\text{CCH}_2\text{S}^i\text{Bu-}t)]$ in the form of a red oil. As independently reported by Lysenko *et al.*, the replacement of the two OH groups in 1 by HSCMe_3 in the presence of HBF_4 gives first the corresponding complex with thioether-substituted acetylene, which was

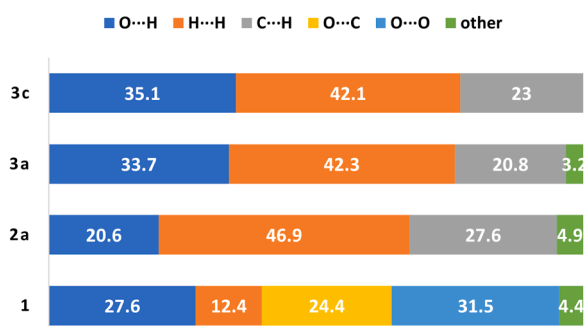


Fig. 10. Plot of percentage contributions of different intermolecular contacts to the Hirshfeld surface of complexes 1, 2a, 3a, and 3c.

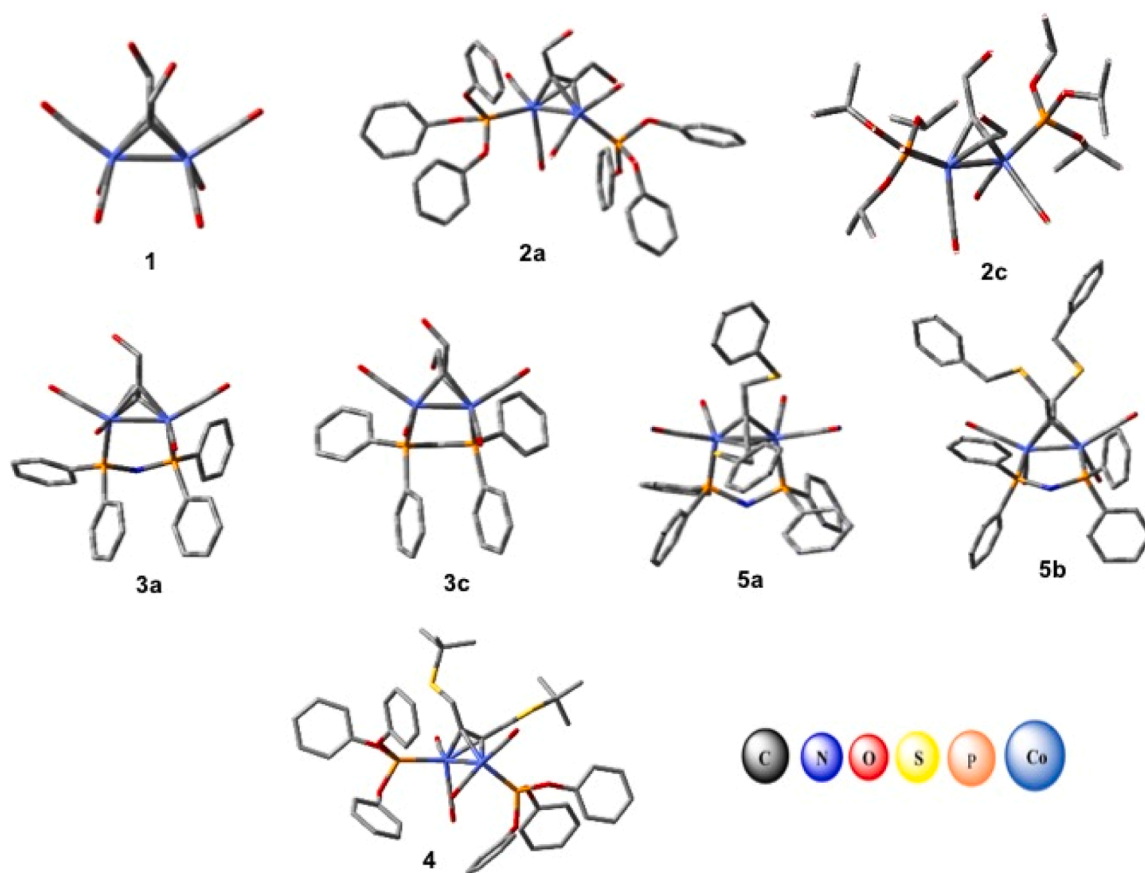


Fig. 11. Optimized structures of investigated homobimetallic complexes at B3LYP/6-31g(d)/LAN12DZ level in the gas phase. The hydrogen atoms are not shown for clarity.

crystallographically characterized as $[(\text{Ph}_3\text{P})\text{Co}_2(\text{CO})_5(\mu-t\text{-BuSCH}_2\text{C}\equiv\text{CCH}_2\text{SBu-t})]$, after substituting for one CO group by PPh_3 [51].

We attempted to convert the phosphite complex $[\text{Co}_2(\text{CO})_4\{\text{P}$

Table 3

Docking score and energy of the Co–Co complexes and prostate cancer proteins (2Q7K and 2AX6).

Comp.	Prostate cancer proteins					
	2Q7K					
	S	rmsd_refine	E_conf	E_place	E_refine	E_score2
1	-4.91	1.60	-452.01	-60.60	29.16	-4.91
2a	-8.88	2.81	159.21	-43.02	-34.15	-8.88
2c	-6.48	2.07	-171.04	-54.49	-27.40	-6.48
3a	-6.11	1.23	44.82	-48.75	-21.34	-6.11
3c	-6.38	2.57	35.26	-42.08	-16.28	-6.38
4	-8.08	4.08	83.65	-27.49	-40.65	-8.08
5a	-7.56	1.94	91.25	-47.29	-37.36	-7.56
5b	-8.66	2.29	94.13	-61.94	-32.04	-8.66

Comp.	2AX6					
	S	rmsd_refine	E_conf	E_place	E_refine	E_score2
1	-5.44	1.16	-456.24	-66.69	68.28	-5.44
2a	-8.83	2.44	159.36	-27.33	-39.09	-8.83
2c	-6.98	1.99	-160.98	-43.15	-24.97	-6.98
3a	-6.66	0.95	47.49	-63.92	-29.82	-6.66
3c	-6.67	1.10	44.25	-44.04	-30.82	-6.67
4	-7.83	3.43	106.02	6.46	-29.54	-7.83
5a	-7.69	2.86	106.79	-40.84	-35.89	-7.69
5b	-8.84	1.89	96.20	-70.96	-28.89	-8.84

S: final score, **E_conf**: Energy of conformation, **Rmsd_refine**: Root mean square deviation of the pose in Å from the original ligand

$(\text{OPh})_3\}_2(\mu\text{-HOCH}_2\text{C}\equiv\text{CCH}_2\text{OH})]$ (**2a**) under these conditions to prepare $[\text{Co}_2(\text{CO})_4\{\text{P}(\text{OPh})_3\}_2(\mu\text{-}t\text{-BuSCH}_2\text{C}\equiv\text{CCH}_2\text{SBu-t})]$ (**5**). Unfortunately, the targeted complex **4** was only obtained in low yield < 10% along with other unidentified compounds (Scheme 2). Therefore, we prepared **4** alternatively by treatment of $[\text{Co}_2(\text{CO})_6\{\text{P}(\text{OPh})_3\}_2]$ with a slight excess of the acetylenic dithioether $t\text{-BuSCH}_2\text{C}\equiv\text{CCH}_2\text{SBu-t}$ [73] in hot toluene and isolated the dimetallatetrahdrene complex in 82% as a red crystalline solid.

Its $^{31}\text{P}\{^1\text{H}\}$ NMR gives rise to a broad singlet at δ 150.5, with $\Delta\delta$ of 1.3 ppm with respect to compound **2a**. Three broad resonances are also present in the ^1H NMR spectrum at δ 1.22, 4.10 and 7.16 ppm, respectively, assigned to $t\text{-Bu}$, SCH_2 , and phenyl groups. In the ^{13}C NMR spectrum, signals corresponding to the thioalkyne part appear as singlets at δ 42.2 (CMe_3), 33.1 (SCH_2), 31.1 (CH_3), 91.8 ppm for the tetrahedrane carbons and the four CO give rise to a sole signal at δ 203.3 ppm. In the aromatic region, two sets of singlets are observed for all the phenyl ring carbons, and this does not evolve when the spectrum is recorded at 323 K. These results suggest that inequivalent phenyl rings are present in compound **4** (Fig S5).

An X-ray diffraction study allowed us to elucidate the molecular structure of this cluster compound crystallizing in the triclinic space group $P-1$ (Table S1). The Co–Co bond distance between the two crystallographic non-equivalent metal centers is elongated with respect to that of $[\text{Co}_2(\text{CO})_4\{\text{P}(\text{OPh})_3\}_2(\mu\text{-HOCH}_2\text{C}\equiv\text{CCH}_2\text{OH})]$ (**2a**) (2.47975 (19) vs. 2.4588(17) Å). The principal structural difference between these two compounds concerns the relative orientation of the two $\text{P}(\text{OPh})_3$ ligands. Whereas in **1** the two phosphorous atoms point in the same directions toward the bridging alkyne with a torsion angle of -43.82° , the phosphorous atoms of **4** point in opposite directions with a torsion angle of 133.89° . P1 is in a pseudo axial position while P2 is in a pseudo

Table 4
Interaction table between the metal complexes and prostate cancer proteins.

Protein	Compound	Ligand	Receptor	Interaction	Distance (Å)	E (kcal/mol)
2Q7K	2a	No measurable interactions				
	4	O1 6	OE2 GLU681	Ionic	3.21	-3.2
		6-ring	NH1 ARG752	pi-cation	3.78	-1.0
2AX6	5b	S005 5	ND2 ASN756	H-acceptor	3.51	-2.0
	2a	6-ring	CB PRO682	pi-H	4.85	-0.5
		No measurable interactions				
2AX6	4	6-ring	VAL684	pi-H	4.81	-0.5
	5b	No measurable interactions				

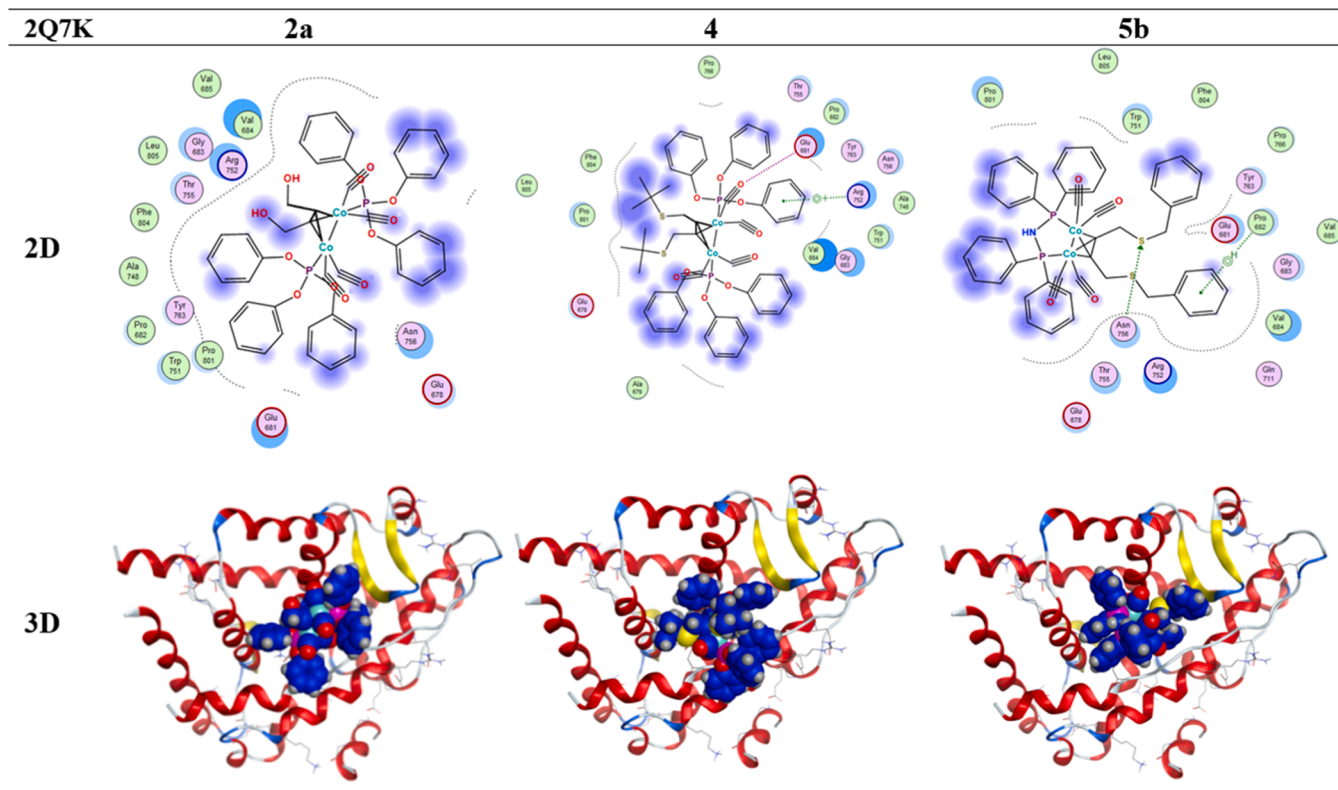


Fig. 12. 2D and 3D docking interaction between complexes **2a**, **4**, **5b** and prostate cancer protein (PDB: 2Q7K).

equatorial one with CoP distances $d(\text{Co1-P1})$ 2.12310(15) Å and $d(\text{Co2-P2})$ 2.1643(20) Å. In **2a**, the cobalt-phosphorous bond lengths are $d(\text{Co1-P1})$ 2.1297(2) and $d(\text{Co2-P2})$ 2.1159(20) Å so these values show a significant elongation of the Co-P_{eq} bond distance relatively to the Co-P_{ax}. This trend is also observed in $\text{Co}_2(\text{CO})_6(\mu\text{-RC}\equiv\text{CR}')$ complexes, where the mean Co-C_{eq} bond length of the four pseudo-equatorial carbonyls is somewhat longer than that of the two pseudo-axial CO ligands. For example, these values are 1.825(3) and 1.805(3) Å, respectively in compound **1**. The XRD corroborates the ¹³C NMR data showing the inequivalence of the phosphorous phenyl rings, which are probably favored by the presence of the bulky *t*-Bu groups. Despite one axial and one equatorial phosphite in **4**, which implies a loss of symmetry compared to the diaxial **2a** phosphite compound (Fig. 6), the ATR-IR spectra in the solid state are similar in the carbonyl region. Four absorptions are observed in the same range with a notable difference in the relative intensities (Fig. S6).

2.7. Synthesis and crystal structure of $[\text{Co}_2(\text{CO})_4(\mu\text{-dppa})_2(\mu\text{-PhSCH}_2\text{C}\equiv\text{CCH}_2\text{SPh})]$ (**5a**) and $[\text{Co}_2(\text{CO})_4(\mu\text{-dppa})_2(\mu\text{-BzSCH}_2\text{C}\equiv\text{CCH}_2\text{SBz})]$ (**5b**)

Upon treatment of $[\text{Co}_2(\mu_2\text{-CO})_2(\text{CO})_4(\mu\text{-dppa})]$ with 1,4-bis

(phenylthio)but-2-yne $\text{PhSCH}_2\text{C}\equiv\text{CCH}_2\text{SPh}$ [74] in warm toluene, the complex $[\text{Co}_2(\text{CO})_4(\mu\text{-dppa})_2(\mu\text{-PhSCH}_2\text{C}\equiv\text{CCH}_2\text{SPh})]$ (**5a**) was formed straight forwardly and isolated in form of red crystals (Scheme 2). Unfortunately, the quality of the crystallographic data was quite poor due to disorder and other problems, so a structural discussion seems inappropriate. However, the atom connectivity could be ascertained, and the non-refined structure is shown in Fig. S7 in the supporting information. The complex $[\text{Co}_2(\text{CO})_4(\mu\text{-dppa})_2(\mu\text{-BzSCH}_2\text{C}\equiv\text{CCH}_2\text{SBz})]$ (**5b**) is formed as an outcome of the reaction with the benzyl derivative $\text{BzSCH}_2\text{C}\equiv\text{CCH}_2\text{SBz}$ [75] under identical condition (Scheme 2). The molecular structure of **5b** is shown in Fig. 8 (Table S2). The asymmetric unit contains two independent molecules whose overall architecture is similar to that of $[\text{Co}_2(\text{CO})_4(\mu\text{-dppa})_2(\mu\text{-HOCH}_2\text{C}\equiv\text{CCH}_2\text{OH})]$ (**3a**) and other dppa-spanned dimetallatetrahedranes discussed above. The Co1-Co2 bond length matches with that of **3a** (2.4520(8) vs. 2.4499(7) Å), the distance of the orthogonal arranged C1-C2 bond (with respect to the Co-Co vector) is considerably lengthened with respect to that of free $\text{BzSCH}_2\text{C}\equiv\text{CCH}_2\text{SBz}$ (1.346(2) vs. 1.193(3) Å) [75]. Several intermolecular interactions involve the heteroatoms and the methylene or aromatic groups, and many H...C contacts are also identified in the supramolecular structure. The amino groups of the two independent molecules give rise to very weak O1...H2N2¹ and N1H1...O5²

Table 6

Interaction table between the metal complexes and breast cancer proteins.

Protein	Compound	Ligand	Receptor	Interaction	Distance (Å)	E (kcal/mol)
1HK7	2a	O2 7	NZ LYS338	H-acceptor	3.02	-4.8
		6-ring	CB PHE332	pi-H	3.75	-0.7
		6-ring	NZ LYS338	pi-cation	3.20	-0.5
	5b	S005 5	ND2 ASN340	H-acceptor	3.17	-2.7
		S005 5	CE LYS366	H-acceptor	3.38	-1.0
		S006 82	NZ LYS338	H-acceptor	3.72	-1.7
		O007 6	OD2 ASP352	Ionic	3.94	-0.6
		O00A 9	OD1 ASP330	Ionic	2.67	-7.1
		6-ring	CB ASN298	pi-H	3.88	-0.5
3EQM	2a	O1 5	NH2 ARG115	H-acceptor	2.77	-5.9
		Co2 2	NH2 ARG115	Ionic	2.78	-6.1
	5b	6-ring	CE2 PHE 430	pi-H	4.09	-0.8

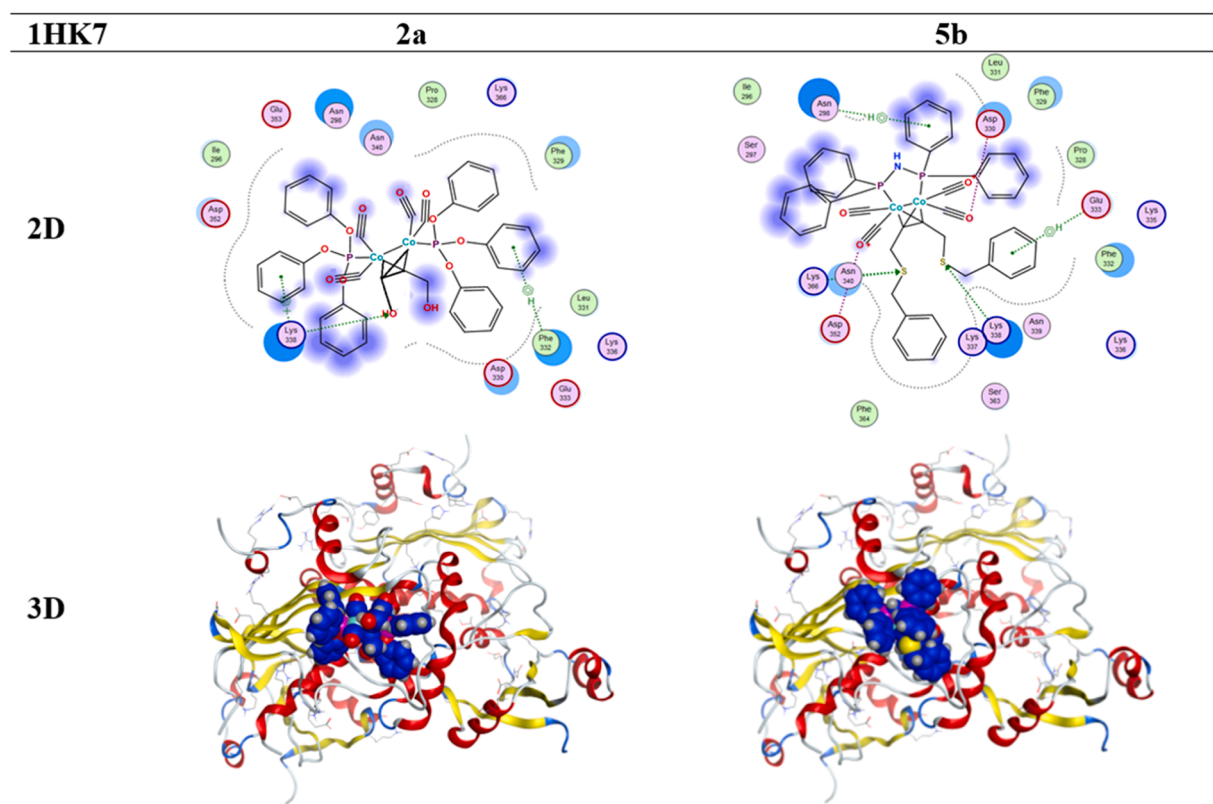


Fig. 14. 2D and 3D docking interaction between complexes 2a, 5b and breast cancer protein (PDB: 1HK7).

interactions, which are dominating in 2a, 3a, and 3c. In 2a, the percentage of O...H contacts is the lowest, probably resulting from the lack of hydrogen bonding (see above). Compared to complex 1, the O...H interactions are significantly higher in the compound 3 bearing a bridging dppa or dppm ligand. This is consistent with the structural description of the packing arrangement.

2.4. DFT calculations conducted on selected dicobalt structures

Several theoretical studies have been carried out on alkyne-bridged dicobalt hexacarbonyl species to analyse electronic distribution, structure and energy of such complexes as well as their reactivity in the Pauson-Khand reaction [46,78–81]. DFT calculations were performed on 1, 2a, 2c, 3a, 3c, 4, and 5a-b to optimize the ground state structure in the gas phase. The DFT-optimized geometries are shown in Fig. 11 and selected calculated (DFT) and experimental (XRD) geometric parameters are compared in Table 2. The concordance between the

calculated values and the experimental data is quite satisfactory for most compounds. One exception concerns the Co–Co–P angle of 2a. Furthermore, 4 presents an optimized molecular geometry different from that established by SCXRD (see Fig. 7). Computational studies indicate the presence of two diaxial arranged phosphites and 4 equatorial carbonyl groups. This divergence may be due to the packing effect in the solid state while the optimized geometry is determined in the gas phase.

The frontier orbitals HOMO and LUMO of 1, 2a, 2c, 3a, 3c, 4, 5a, and 5b and calculated energy gaps ($E_g = E_{LUMO} - E_{HOMO}$) are illustrated in Fig. S16. These molecular orbitals are largely distributed over the Co_2C_2 tetrahedrane core in all complexes as observed for $Co_2(CO)_6(\text{-nucleoside})$ [39,82]. The frontier molecular orbital energies (E_{HOMO} , E_{LUMO}) are presented in Fig. S17 and additional calculated data are presented in Table S3. The HOMO-LUMO gap for all the compounds is in the range 3.53 - 4.03 eV. These values are superior to that reported by Kaczmarek for a dicobalt hexacarbonyl modified nucleoside with a

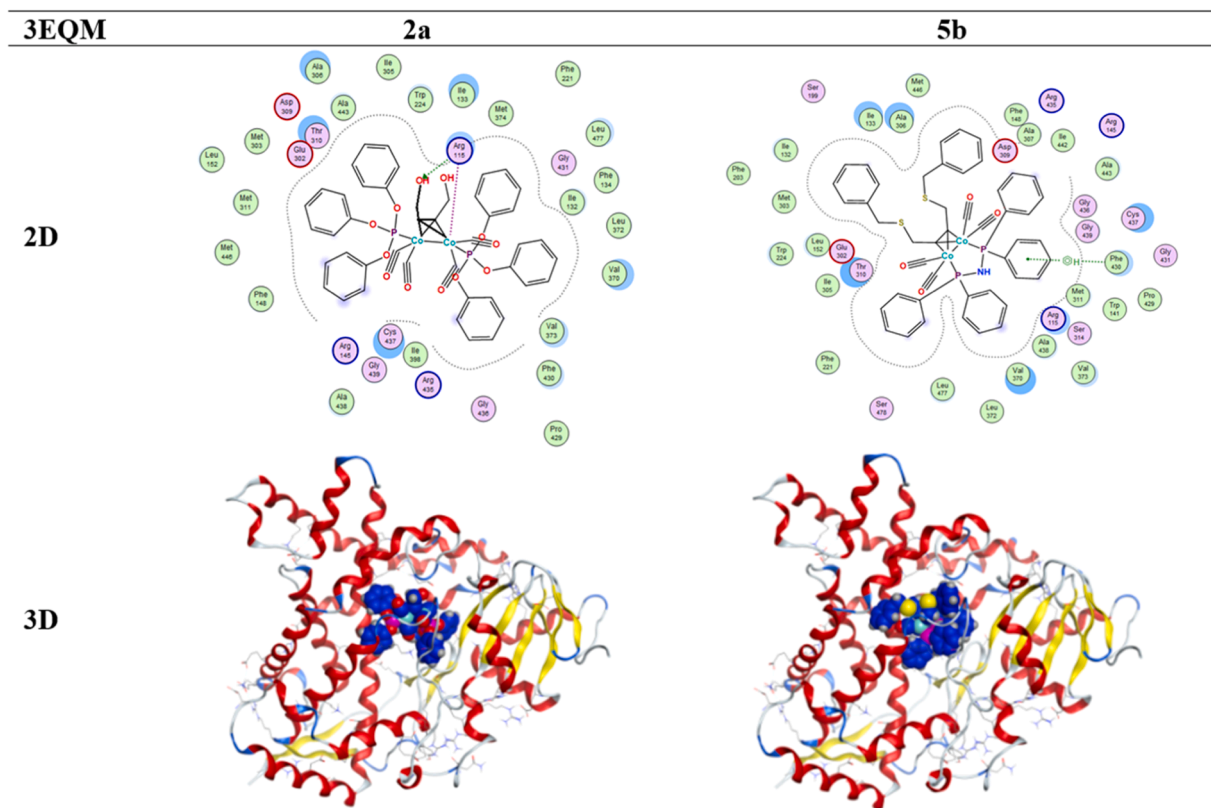


Fig. 15. 2D and 3D docking interactions between complexes 2a, 5b and breast cancer protein (PDB: 3EQM).

Table 7

Docking score and energy of the cobalt-cobalt complexes and liver cancer proteins (4FM9).

comp	Liver cancer protein					
	4FM9					
	S	rmsd_refine	E_conf	E_place	E_refine	E_score2
1	-5.75	0.96	-481.33	-88.63	50.67	-5.75
2a	-9.74	3.87	173.95	-71.34	-53.24	-9.74
2c	-8.80	2.03	-119.72	-55.67	-27.38	-8.80
3a	-7.16	1.88	53.26	-65.66	-26.44	-7.16
3c	-7.07	1.44	54.00	-69.16	-15.16	-7.07
4	-10.97	2.22	133.80	-78.53	-47.28	-10.97
5a	-8.36	2.54	101.72	-60.44	-34.60	-8.36
5b	-9.42	2.01	103.18	-56.31	-22.84	-9.42

S: final score, E_conf: Energy of conformation, Rmsd_refine: Root mean square deviation of the pose in Å from the original ligand

calculated energy gap of 3.12 eV using DFT/B3LYP/6-31G* [82].

Molecular Electrostatic Potential (MEP) maps for **1**, **2a**, **2c**, **3a**, **3c**, **4**, **5a**, and **5b** were also determined (Fig. S18) to locate the electron density in the dicobalt tetrahedrane complexes. The red areas on the MEP map indicate regions of negative electrostatic potential. They are typically associated with electron-rich areas of the molecule, such as lone pairs of electrons or atoms with high electronegativity. These regions are likely to be nucleophilic and attract positively charged species. The blue areas represent regions of positive electrostatic potential, indicating electron-deficient areas. Typically, these regions are associated with hydrogen atoms or other less electronegative atoms. These areas are electrophilic and tend to attract negatively charged species. As expected, the minimum electrostatic potentials (red-orange-yellow colored area) are focused on the O and S atoms of terminal carbonyl, hydroxyl or thioether groups of the complexes. Electron deficient regions are located on the hydrogen of the OH function for the BUD derivatives. Varied

distribution and intensity of the colored area on the phosphane substituted dicobalt tetrahedrane could favor the ligand-protein interactions.

2.5. Molecular docking of dicobalt complexes

Docking studies allow to estimate interactions between guest compounds and the active site of biomolecules such as proteins or DNA (host). This helps in understanding binding affinities and the potential efficacy of target compounds before experimental validation, saving considerably time and resources. This approach allows the screening of large libraries of compounds to identify promising candidates for further development. Docking simulations can be used iteratively to optimize lead compounds by modifying their structure to improve binding affinity and specificity for the target protein. Docking is also a crucial component of structure-based drug design, where it helps in designing new molecules with improved binding characteristics based on the three-dimensional structure of the target protein. Furthermore, docking can predict multiple binding modes of a ligand to a target, providing insight into possible conformational flexibility and alternate binding sites, which can be valuable for understanding allosteric regulation or designing multi-target drugs [83-91].

The anticancer activity of $\text{Co}_2(\text{CO})_6(\text{alkyne})$ tetrahedranes as carbon monoxide releasing molecules (CORMs) has been previously evaluated *in silico* using the COX-2 protein (PDB: 5FA1) [92]. We have recently published an *in silico* study on the heterometallic diphosphine-spanned complexes $[(\text{OC})_2\text{Fe}(\mu\text{-dppm})\{\mu\text{-C}(=\text{O})\text{C}(\text{CH}_2)_3\text{OH}=\text{CH}\}\text{Pt}(\text{PPh}_3)_3]$, $[(\text{OC})_2\text{Fe}(\mu\text{-dppm})\{\mu\text{-C}(=\text{O})\text{C}(\text{CH}_2\text{CH}(\text{OH})\text{CH}_3)=\text{CH}\}\text{Pt}(\text{PPh}_3)_3]$, and $[(\text{OC})_2\text{Fe}(\mu\text{-dppm})\{\mu\text{-C}(=\text{O})\text{C}(\text{CH}_2\text{S}(p\text{-tolyl}))=\text{C}(\text{CH}_2\text{S}(p\text{-tolyl}))\}\text{Pt}(\text{PPh}_3)_3]$ to evaluate their anticancer activity. Like diphosphine-spanned compounds **3** and **5**, the latter crystallographically characterized Fe-Pt complexes have been obtained by treatment of the bimetallic starting complexes with the appropriate alkynol or thioether-functionalized alkyne. For this purpose, specifically proteins responsible for prostate

and breast cancer have been chosen [57]. To compare with the activity of the homobimetallic dicobalt complexes, we have performed simulations with the same proteins and also with a liver cancer protein.

2.5.1. Prostate cancer proteins (2Q7K and 2AX6)

We were now curious, whether the above described dicobalt tetrahedrane complexes would be more or less potent as potential metalodrugs by comparing their binding score using the same biological environment. Specifically, two proteins responsible for prostate cancer, namely 2Q7K (www.rcsb.org/structure/2q7k) and 2AX6 (www.rcsb.org/structure/2AX6), have been chosen. Recently, similar docking studies against 2Q7K were carried out using 6-aminopenicillanic acid [93]. In the context of prostate cancer treatment, *in silico* docking analyses of 5,5-dimethylthiohydantoin derivatives as androgen antagonist have been screened against 2AX6 [94]. The herein presented *in silico* evaluation of the dicobalt tetrahedrane complexes revealed globally a favorable biological response to complex-protein interactions. As detailed below, the results of low binding energy vary between -4.91 and -8.88 kcal/mol for the 2Q7K and between -5.44 and -8.84 kcal/mol for the 2AX6 proteins (Table 3).

Compounds **2a**, **5b**, and **4** present the best interaction energy score with -8.88, -8.66, and -8.08 kcal/mol, respectively for the 2Q7K protein (Table 3). The remaining compounds exhibit less important interactions in the -7.56 and -4.91 kcal/mol range. Although compound **2a** has no measurable interactions with the receptor (Table 4), it gave the best score of -8.88 kcal/mol with the 2Q7K protein (Fig. 12). Its binding energy against 2Q7K is clearly superior compared to the binding energy values obtained for the heterobimetallic complexes $[(OC)_2Fe(\mu-dppm)\{\mu-C(=O)C(CH_2)_3OH=CH\}Pt(PPh_3)]$, $[(OC)_2Fe(\mu-dppm)\{\mu-C(=O)C(CH_2CH(OH)CH_3)=CH\}Pt(PPh_3)]$, and $[(OC)_2Fe(\mu-dppm)\{\mu-C(=O)C(CH_2S(p-tolyl))=C(CH_2S(p-tolyl))\}Pt(PPh_3)]$ (-7.77, -7.05, and -8.62 kcal/mol, respectively) [57]. Complex **5b** interacts with ASN756 and PRO682 through hydrogen bonding and π -H interaction involving a sulfur atom and a phenyl group from the dithioether moiety. In compound **4**, ionic interactions involve CO and P(OPh)₃ substituents with GLU681 and ARG752.

Compounds **5b**, **2a**, and **4** also formed better complex-2AX6 interactions with -8.84, -8.83, and -7.83 kcal/mol, respectively (Table 3). The free binding energies remain of the same order of magnitude as the complex-2Q7K interactions. Note that the *in silico* response between **2a**-2AX6 and **5b**-2AX6 (-8.83 vs -8.84 kcal/mol), are quite close (Fig. 13).

For the 2AX6 protein, the bond energies are of the same order of magnitude as for the complexes $[(OC)_2Fe(\mu-dppm)\{\mu-C(=O)C(CH_2)_3OH=CH\}Pt(PPh_3)]$ and $[(OC)_2Fe(\mu-dppm)\{\mu-C(=O)C(CH_2S(p-tolyl))=C(CH_2S(p-tolyl))\}Pt(PPh_3)]$ (-8.19 and -8.26 kcal/mol respectively) whereas for $[(OC)_2Fe(\mu-dppm)\{\mu-C(=O)C(CH_2CH(OH)CH_3)=CH\}Pt(PPh_3)]$ (-7.57 kcal/mol) it is somewhat weaker [57]. Note that despite good docking scores, no measurable interactions were detected between **2a**, **5b** and the receptor.

The bonding pose of other complexes in 2Q7K and 2AX6 proteins and their interactions are presented in Tables S4-S5.

2.5.2. Breast cancer proteins (1HK7 and 3EQM)

Oxidovanadium(IV) complexes were recently screened for their anticancer activity against breast adenocarcinoma (MCF-7) using docking studies against 1HK7 (www.rcsb.org/structure/1HK7) [95]. Molecular docking studies were also performed with the aromatase enzyme present in the breast tissues (PDB ID 3EQM) (www.rcsb.org/structure/3EQM) revealing binding interactions of novel organic 1,3,4-oxadiazole-benzimidazole with the receptor active sites [96]. With

this in mind, compounds **1**, **2a**, **2c**, **3a**, **3c**, **4**, and **5a-b** were also evaluated for their effectiveness against the proteins involved in breast cancer, namely 1HK7 and 3EQM (Tables S6-S7). The low binding energies vary between -4.71 and -8.99 kcal/mol for the complex-1HK7 structures and between -5.78 and -11.01 kcal/mol for the complex-3EQM (Table 5).

As before, complexes **2a** and **5b** have the highest binding scores with -8.99 and -8.93 kcal/mol, respectively, with the 1HK7 protein (Tables 5-6, Fig. 14). Complex **2a** shows the best affinity through various interactions with the amino acids of the 1HK7 protein. A hydrogen bonding between a hydroxyl function of BUD and LYS338 is observed with a bond length of 3.02 Å, while P(OPh)₃ groups are involved in π -interactions with PHE332 and LYS338 amino acids. The free binding energy determined for **5b**-1HK7 is quite close and 7 interactions are detected between **5b** and the protein. The sulfur atoms give rise to hydrogen bonds with ASN340, LYS338 and LYS366, and π -interactions with ASP330 and ASN398 are observed with the aromatic cycles of dppa and a thiobenzyl group as well as ionic interactions between carbonyls and ASP330, ASN352.

The free binding energies recorded of **2a**-1HK7 and **5b**-1HK7 are slightly higher than the free binding energies of the heterobimetallic alkynol compounds $[(OC)_2Fe\{\mu-dppm\}\{\mu-C(=O)C(CH_2)_3OH=CH\}Pt(PPh_3)]$ (-8.52 kcal/mol) and $[(OC)_2Fe\{\mu-dppm\}\{\mu-C(=O)C(CH_2CH(OH)CH_3)=CH\}Pt(PPh_3)]$ (-8.66 kcal/mol). However for the dithioether compound $[(OC)_2Fe(\mu-dppm)\{\mu-C(=O)C(CH_2S(p-tolyl))=C(CH_2S(p-tolyl))\}Pt(PPh_3)]$, a weaker docking score of -7.61 kcal/mol was determined with the 1HK7 protein resulting only from a π -cation interaction of a *S-p*-tolyl cycle with LYS338 [57].

Concerning the complexes-3EQM affinity, the docking scores are in the same order of magnitude, and range between -9.83 to -11.01 kcal/mol. The only exception is $[(OC)_6Co_2(\mu-HOCH_2C\equiv CCH_2OH)]$ (**1**) with a lower binding energy value of -5.78 kcal/mol (Table 5). All the complexes exhibit a good affinity and the best binding energies with this protein. This could be explained by the structure of the 3EQM receptor, allowing an easier access to the host molecule. The binding site interactions of the lead compounds **2a** and **5b** with the 3EQM target are presented Fig. 15 and Table 6. In the active site, the amino acid ARG115 has close interactions with a cobalt atom and an OH function of **2a** while a π -interaction involves only a phenyl group of the dppa moiety in **5b** and the PHE430 residue. Except $[(OC)_6Co_2(\mu-C(CH_2OH)\equiv C(CH_2OH))]$ (**1**), the results obtained for the dicobalttetrahedrane show interaction energy values with the 3EQM protein that exceed those determined than for iron-platinum heterobimetallic complexes, namely $[(OC)_2Fe\{\mu-dppm\}\{\mu-C(=O)C(CH_2CH(OH)CH_3)=CH\}Pt(PPh_3)]$ (-9.64 kcal/mol), $[(OC)_2Fe\{\mu-dppm\}\{\mu-C(=O)C(CH_2)_3OH=CH\}Pt(PPh_3)]$ (-9.35 kcal/mol), and $[(OC)_2Fe(\mu-dppm)\{\mu-C(=O)C(CH_2S(p-tolyl))=C(CH_2S(p-tolyl))\}Pt(PPh_3)]$ (-6.8 kcal/mol) [57].

The bonding pose of complexes **1**, **2c**, **3a**, **3c**, **4** and **5a** in the selected breast cancer proteins and their interactions are presented in Tables S6-S7. Docking simulations with the biological target 3EQM have been reported for mononuclear cobalt(II) complexes derived from D-luciferin and 6-mercaptopurin with the respective binding energy values of -9.44 and -6.08 kcal/mol [97,98]. A cobalt(III)-thiourea complex was also evaluated towards breast and prostate cancers using other receptors PDB-3ERT (breast) and PDB-1Z95 (prostate) with docking scores of -9.40 and -8.79 kcal/mol [99].

2.5.3. Liver cancer proteins (4FM9)

Interactions between monofunctional pyridine platinum(II) complexes and DNA topoisomerases which are important targets for DNA-

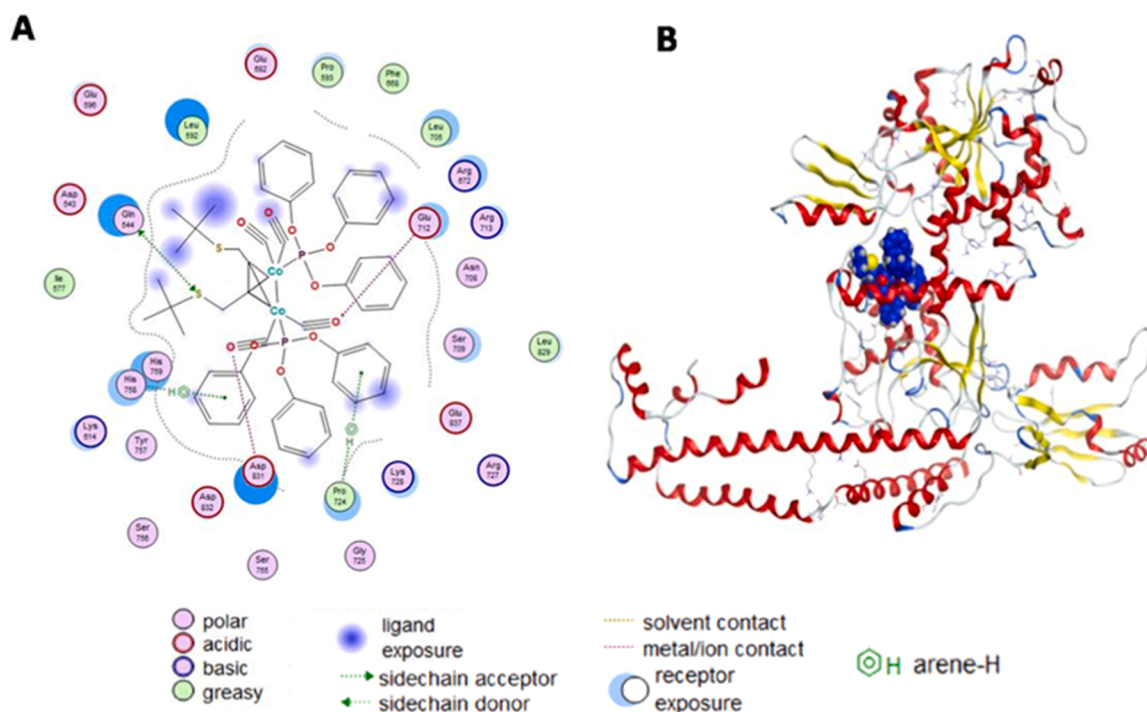


Fig. 16. (A) 2D and (B) 3D docking interaction between the complex 4 and liver cancer protein (PDB: 4FM9).

oriented anticancer drugs were studied using molecular docking with 4FM9. The 4FM9 protein is acting as Type IIA topoisomerases which is essential in the separation of entangled daughter strands during replication. This function is believed to be performed by topoisomerase II in eukaryotes and by topoisomerase IV in prokaryotes. Failure to separate these strands leads to cell death [100,101].

Several studies have also been carried out evaluating organic compounds *in silico* using the 4FM9 protein as receptor, for example thio-uracil based dihydro-indenopyridopyrimidines and fluoroquinolones [102,103]. So, the bimetallic dicobalt complexes were finally tested with this liver cancer protein (www.rcsb.org/structure/4FM9) [104]. The binding energies vary between -5.75 and -10.97 kcal/mol and the affinity of $[\text{Co}_2(\text{CO})_4\{\text{P}(\text{Oph})_3\}_2(\mu-t\text{-BuSCH}_2\text{C}\equiv\text{CCH}_2\text{SBu}-t)]$ (4) towards the receptor is greater than that of 2a and 5b, with values of -10.97, -9.74, and -9.42 kcal/mol, respectively (Table 7).

The results of the molecular docking simulation for 4-4FM9 are presented in Fig. 16 and Table 8 (for the other complexes, see Tables S8-S9). Six interactions are determined between complex 4 and 4FM9 including hydrogen bonding between a sulfur atom and the amino acid GLN544, two ionic interactions between terminal carbonyls and the residues ASP831 and GLU712. Two phenyl cycles of a P(Oph)₃ substituent give rise to π -H interactions with the amino acids PRO724 and HIS758.

For comparison, interactions between 4FM9 receptor and monometallic cobalt(II) bearing *D*-luciferin, 6-mercaptopurin and 2-(2-hydroxybenzoyl)-*N*-phenylhydrazine-1-carbothioamide were studied by molecular docking. The obtained free binding energy values were -8.02,

Table 8

Interaction table between complex and liver cancer protein (PDB: 4FM9).

Protein	Compound	Ligand	Receptor	Interaction	Distance (Å)	E (kcal/mol)
4FM9	4	S2 3	OE1 GLN544 (A)	H-donor	3.85	-0.7
		S2 3	NE2 GLN544 (A)	H-acceptor	3.52	-3.8
		O1 6	OD2 ASP831 (A)	Ionic	2.53	-8.5
		O2 7	OE1 GLU712 (A)	Ionic	2.74	-6.4
		6-ring	CB PRO724 (A)	pi-H	3.77	-0.7
		6-ring	CD2 HIS758 (A)	pi-H	3.73	-0.5

Table 9

Docking scores obtained for the dicobalt complexes and the cancer proteins (kcal/mol)

Comp.	Prostate		Breast		Liver
	2Q7K	2AX6	1HK7	3EQM	4FM9
1	-4.91	-5.44	-4.71	-5.78	-5.75
2a	-8.88	-8.83	-8.99	-11.01	-9.74
2c	-6.48	-6.98	-6.37	-9.86	-8.80
3a	-6.11	-6.66	-6.31	-10.09	-7.16
3c	-6.38	-6.67	-6.22	-10.20	-7.07
4	-8.08	-7.83	-7.63	-9.83	-10.97
5a	-7.56	-7.69	-6.55	-10.22	-8.36
5b	-8.66	-8.84	-8.93	-10.96	-9.42

-5.85 and -6.69 kcal/mol, respectively [97,98,105]. The binding ability of cobalt(II) terpyridine complexes with another DNA-topoisomerase (PDB: 1T8I) has also been investigated *in silico*, showing good affinity ranging from -7.71 to -12.61 kcal/mol [106].

Table 9 summarizes the binding scores obtained for all the tested complexes towards the five proteins chosen as targets for the simulations. It appears that $[(\text{OC})_6\text{Co}_2(\mu\text{-HOCH}_2\text{C}\equiv\text{CCH}_2\text{OH})]$ (1) always presents the lowest affinity whatever the protein. This study reveals that the three lead compounds are phosphine-substituted $[\text{Co}_2(\text{CO})_4\{\text{P}(\text{Oph})_3\}_2(\mu\text{-HOCH}_2\text{C}\equiv\text{CCH}_2\text{OH})]$ (2a), $[\text{Co}_2(\text{CO})_4(\mu\text{-dppa})_2(\mu\text{-BzSCH}_2\text{C}\equiv\text{CCH}_2\text{SBz})]$ (5b) and $[\text{Co}_2(\text{CO})_4\{\text{P}(\text{Oph})_3\}_2(\mu\text{-}t\text{-BuSCH}_2\text{C}\equiv\text{CCH}_2\text{SBu}-t)]$ (4).

3. Conclusion

This study presented the synthesis, spectroscopic, and crystallographic characterization of airstable cobalt-cobalt tetrahedrane complexes ligated by butynediol and various monodentate or bidentate phosphane ligands. The crystallographically evidenced formation of intramolecular seven-membered cycles through H-O•••••H-O bonding was also assessed by Hirshfeld surface analysis performed on the butynediol complexes **1** and **3a**. More extended supramolecular secondary interactions generating supramolecular networks were identified for the diphosphine-spanned $[\text{Co}_2(\text{CO})_4(\mu\text{-dppa})(\mu\text{-HOCH}_2\text{C}\equiv\text{CCH}_2\text{OH})]$ (**3a**), $[\text{Co}_2(\text{CO})_4(\mu\text{-Medppa})(\mu\text{-HOCH}_2\text{C}\equiv\text{CCH}_2\text{OH})]$ (**3b**) and $[\text{Co}_2(\text{CO})_4(\mu\text{-dppm})(\mu\text{-HOCH}_2\text{C}\equiv\text{CCH}_2\text{OH})]$ (**3c**). Furthermore, we have crystallographically analyzed a series of $[\text{Co}_2(\text{CO})_4\text{L}_2(\mu\text{-RSCH}_2\text{C}\equiv\text{CCH}_2\text{SR})]$ complexes, in which the -OH hydroxyl groups are replaced by -SR thioether functions. DFT calculations were employed to determine the optimized geometries of some complexes to compute their HOMO-LUMO gap and the electron density distribution around the homobimetallic scaffold. Most of the optimized geometries match with those obtained by SCXRD, but in some case a divergence between theoretical and experimentally data is apparent, which may be due to packing effect and other secondary interactions occurring in the crystal. The efficacy against breast, prostate, and liver cancers was evaluated *in silico* by molecular docking simulations, providing information on the intermolecular interactions between the metal complexes and the five target proteins 2Q7K, 2AX6, 1HK7, 3EQM and 4FM9 chosen for these three cancer types. This preliminary work reveals encouraging results in relation to intermolecular interactions between diverse protein sites and complexes. In contrast to our initial expectation, the host-guest interactions are not dominated by hydrogen bonding between the OH group of Co-coordinated BUD and the protein residues as receptors, but by other secondary interactions such as $\pi\bullet\bullet\bullet\bullet\text{H}$, $\text{H}\bullet\bullet\bullet\bullet\text{acceptor}$, $\pi\text{-cationic}$ and ionic ones. Whatever the protein target, complexes **2a** (-8.83 to -11.01 kcal/mol), **5b** (-8.66 to -10.96 kcal/mol), and **4** (-7.83 to -10.97 kcal/mol) ligated by P-donor ligands displayed the best docking scores. In contrast, BUD hexacarbonyl complex **1** (-4.71 to -5.78 kcal/mol) was the less potent candidat, indicating the importance of the P-donor ligands for obtaining satisfying docking scores. These $\text{P}(\text{OAr})_3$ or diphosphine-spanned dimetallahedranes represent potential candidates for future homobimetallic metallodrugs against prostate, breast, and liver cancers after an obviously broad study of advanced *in vitro*, *in vivo* and toxicity tests.

4. Experimental section

4.1. Materials and product

$[\text{Co}_2(\text{CO})_8]$, 2-butyne-1,4-diol, $\text{Ph}_2\text{PCH}_2\text{PPh}_2$, $\text{P}(\text{O}i\text{-Pr})_3$, *t*-BuSH were commercially obtained from Acros, Alfa Aesar, Aldrich and TCI. All reactions were performed in Schlenk-tube flasks under purified nitrogen. Solvents were dried and distilled under nitrogen before use. Infrared spectra were recorded on a Bruker Vertex 70 spectrometer using a Platinum ATR accessory equipped with a diamond crystal or on a Bruker Alpha II IRTF spectrometer in solution. The ^1H , $^{13}\text{C}\{^1\text{H}\}$ and $^{31}\text{P}\{^1\text{H}\}$ NMR spectra were obtained on a Bruker Avance 400 HD instrument at 400, 100.62 and 121.50 MHz, respectively using CDCl_3 as solvent unless otherwise stated. ^1H chemical shifts were referenced to the proton impurity of the NMR solvent and ^{13}C chemical shifts to the NMR solvent. Elemental analyses were performed on a Thermo Fisher Flashsmart CHNS elemental analyzer by SynBioN (Université de Lorraine-CNRS).

4.2. Synthesis

The cobalt carbonyl complexes $[\text{Co}_2(\text{CO})_6(\mu\text{-dppm})]$, $[\text{Co}_2(\text{CO})_6(\mu\text{-dppa})]$, $[\text{Co}_2(\text{CO})_6\{\text{P}(\text{O}i\text{-PrO})_3\}_2]$ and $[\text{Co}_2(\text{CO})_6\{\text{P}(i\text{-PrO})_3\}_2]$ were

synthesized according procedures described in the literature [58,63,66]. $[\text{Co}_2(\text{CO})_6(\mu\text{-HOCH}_2\text{C}\equiv\text{CCH}_2\text{OH})]$ (**1**) and $[(\text{OC})_4\text{Co}_2(\mu\text{-dppa})(\mu\text{-C}(\text{CH}_2\text{OH})\equiv\text{C}(\text{CH}_2\text{OH}))]$ (**3a**) were synthesized according to slightly modified procedures described by Gruselle [47] and Ellermann [66] using toluene as solvent. The dithioethers ligands 1,4-bis(*t*-butylthio)but-2-yne, 1,4-bis(phenylthio)but-2-yne and 1,4-bis(benzylthio)but-2-yne were prepared as previously reported [73-75].

General procedure to synthesize the bis(phosphine) $\text{Co}_2(\text{CO})_4(\mu\text{-RCH}_2\text{C}\equiv\text{CCH}_2\text{R})$ tetrahedranes

An equimolar amount of alkyne (0.2 mmol) was added to a stirred solution of the bis(phosphine)dicobalt hexacarbonyl complex (0.2 mmol) in 5 mL of toluene. The reaction mixture was heated at 60°C for few hours, following the reaction using IR spectroscopy. The solvent was subsequently evaporated and the residue was then dried under vacuum before recrystallization in toluene/heptane.

Synthesis of $[\text{Co}_2(\text{CO})_4\{\text{P}(\text{OPh})_3\}_2(\mu\text{-HOCH}_2\text{C}\equiv\text{CCH}_2\text{OH})]$ (2a**):** From BUD (17 mg, 0.2 mmol) and $[\text{Co}_2(\text{CO})_6\{\text{P}(\text{OPh})_3\}_2]$ (181 mg, 0.2 mmol). Red crystals. Yield: 159 mg, 85%. Anal. Found: C, 56.31; H, 3.77. Calc. for $\text{C}_{44}\text{H}_{36}\text{Co}_2\text{O}_{12}\text{P}_2$ (936.58 g. mol⁻¹): C, 56.43; H, 3.87.

Synthesis of $[\text{Co}_2(\text{CO})_4\{\text{P}(\text{OTol-}o)_3\}_2(\mu\text{-HOCH}_2\text{C}\equiv\text{CCH}_2\text{OH})]$ (2b**):** From BUD (17 mg, 0.2 mmol) and $[\text{Co}_2(\text{CO})_6\{\text{P}(\text{OTol-}o)_3\}_2]$ (181 mg, 0.2 mmol). Red powder. Yield: 153 mg, 75%. Anal. Found: C, 58.75; H, 4.67. Calc. for $\text{C}_{50}\text{H}_{48}\text{Co}_2\text{O}_{12}\text{P}_2$ (1020.74 g. mol⁻¹): C, 58.84; H, 4.74.

Synthesis of $[\text{Co}_2(\text{CO})_4\{\text{P}(\text{OPr-}i)_3\}_2(\mu\text{-HOCH}_2\text{C}\equiv\text{CCH}_2\text{OH})]$ (2c**):** (a) From BUD (17 mg, 0.2 mmol) and $[\text{Co}_2(\text{CO})_6\{\text{P}(\text{OPr-}i)_3\}_2]$ (140 mg, 0.2 mmol). (b) From $[\text{Co}_2(\text{CO})_6(\mu\text{-HOCH}_2\text{C}\equiv\text{CCH}_2\text{OH})]$ (**1**) (74 mg, 0.2 mmol) and $\text{P}(\text{OPr-}i)_3$ (83 mg, 0.4 mmol). Red waxy solid. $\text{C}_{26}\text{H}_{48}\text{Co}_2\text{O}_{12}\text{P}_2$ (732.42 g. mol⁻¹).

Synthesis of $[\text{Co}_2(\text{CO})_4(\mu\text{-Medppa})(\mu\text{-HOCH}_2\text{C}\equiv\text{CCH}_2\text{OH})]$ (3b**):** From $[\text{Co}_2(\text{CO})_8]$ (68 mg, 0.2 mmol), Medppa (80 mg, 0.2 mmol) and BUD (17 mg, 0.2 mmol). Red crystals. Yield: 109 mg, 76%. Anal. Found: C, 55.32; H, 4.03. Calc. for $\text{C}_{33}\text{H}_{29}\text{Co}_2\text{NO}_6\text{P}_2$ (715.41 g. mol⁻¹): C, 55.40; H, 4.09.

Synthesis of $[(\text{OC})_4\text{Co}_2(\mu\text{-dppm})(\mu\text{-HOCH}_2\text{C}\equiv\text{CCH}_2\text{OH})]$ (3c**):** From BUD (17 mg, 0.2 mmol) and $[\text{Co}_2(\text{CO})_6(\mu\text{-dppm})]$ (134 mg, 0.2 mmol). Orange-red needles. Yield: 117 mg, 84%. Anal. Found: C, 56.43; H, 3.98. Calc. for $\text{C}_{33}\text{H}_{28}\text{Co}_2\text{O}_6\text{P}_2$ (700.39 g. mol⁻¹): C, 56.59; H, 4.03.

Synthesis of $[\text{Co}_2(\text{CO})_4\{\text{P}(\text{OPh})_3\}_2(\mu\text{-}t\text{-BuSCH}_2\text{C}\equiv\text{CCH}_2\text{SBu-}t)]$ (4**):** From 1,4-bis(*t*-butylthio)but-2-yne (48 mg, 0.21 mmol) and $[\text{Co}_2(\text{CO})_6\{\text{P}(\text{OPh})_3\}_2]$ (181 mg, 0.2 mmol). Red crystalline solid. Yield: 177 mg, 82%. Anal. Found: C, 57.68; H, 4.78. Calc. for $\text{C}_{52}\text{H}_{52}\text{Co}_2\text{O}_{10}\text{P}_2\text{S}_2$ (1080.93 g. mol⁻¹): C, 57.78; H, 4.85.

Synthesis of $[\text{Co}_2(\text{CO})_4(\mu\text{-dppa})(\mu\text{-PhSCH}_2\text{C}\equiv\text{CCH}_2\text{SPh})]$ (5a**):** From 1,4-bis(phenylthio)but-2-yne (57 mg, 0.21 mmol) and $[\text{Co}_2(\text{CO})_6(\mu\text{-dppa})]$ (136 mg, 0.2 mmol). Red crystalline solid. Yield: 133 mg, 75%. Anal. Found: C, 59.56; H, 3.91. Calc. for $\text{C}_{44}\text{H}_{35}\text{Co}_2\text{NO}_4\text{P}_2\text{S}_2$ (885.71 g. mol⁻¹): C, 59.67; H, 3.98.

Synthesis of $[\text{Co}_2(\text{CO})_4(\mu\text{-dppa})(\mu\text{-BzSCH}_2\text{C}\equiv\text{CCH}_2\text{SBz})]$ (5b**):** From 1,4-bis(benzylthio)but-2-yne (63 mg, 0.21 mmol) and $[\text{Co}_2(\text{CO})_6(\mu\text{-dppa})]$ (136 mg, 0.2 mmol). Red crystals. Yield: 144 mg, 79%. Anal. Found: C, 60.47; H, 4.30. Calc. for $\text{C}_{46}\text{H}_{39}\text{Co}_2\text{NO}_4\text{P}_2\text{S}_2$ (913.77 g. mol⁻¹): C, 60.47; H, 4.30.

4.2. X-ray crystallography

The crystal structure of **1**, **2a**, **3a-c**, **4**, and **5a-b** was determined using a Bruker D8 Venture four-circle diffractometer equipped with a PHOTON II CPAD detector by Bruker AXS GmbH. The X-ray radiation was generated by the $\text{I}\mu\text{S}/\text{I}\mu\text{S}$ microfocus source Mo ($\lambda = 0.71073 \text{ \AA}$) from Incoatec GmbH equipped with HELIOS mirror optics and a single-hole collimator by Bruker AXS GmbH. The selected single crystals were covered with an inert oil (perfluoropolyalkyl ether) and mounted on a MicroMount, MicroLoop or MicroGripper from MiTeGen. The APEX3 Suite (v2018.7-2, v2019.1-0, v2019.11-0) and APEX4 Suite (v.2021.10-0) [107,108] software integrated with SAINT (integration) [109] and

SADABS (adsorption correction) [110] programs by Bruker AXS GmbH were used for data collection. The processing and finalization of the crystal structure were performed using the Olex2 program [111]. The crystal structures were solved by the ShelXT [112] structure solution program using the Intrinsic Phasing option, which were further refined by the ShelXL [113] refinement package using Least Squares minimization. The non-hydrogen atoms were anisotropically refined.

In compound **3b**, H21B was refined freely, as well as all hydrogen atoms in compound **2a**, hydroxy hydrogen atoms H1 and H2 and amine hydrogen atom H1A in compound **3a**. Also, in compound **3c** all hydroxy hydrogen atoms were refined freely. All remaining H atoms were placed in geometrically calculated positions, and a fixed isotropic displacement parameter was assigned to each atom according to the riding model: C–H = 0.95–1.00 Å with Uiso(H) = 1.5 Ueq (CH₃) and 1.2 Ueq (CH₂, CH) for other hydrogen atoms. In compound **5b** one sulfide group is positionally disordered and refined using free variables. The sulfur atom S1 and the carbon atom C50 and C51 were disordered with a ratio of 76:24. In compound **3a** one phenyl ring is positionally disordered and refined using free variables. The carbon atoms C28, C29, and C30 were disordered with a ratio of 50:50. In compound **3b** the hydroxy groups are positionally disordered and refined using free variables. The hydrogen atoms H1, H2, H7, and H8 were disordered with a ratio of 54:46.

The crystallographic data for the structures of **1**, **2a**, **3a**, **3b**, **3c**, **4**, as well as for **5b** have been published as supplementary publication number 2342036 (**1**), 2342038 (**2a**), 2342039 (**3a**), 2342041 (**3b**), 2342037 (**3c**), 2343180 (**4**), 2342040 (**5b**) in the Cambridge Crystallographic Data Centre. A copy of these data can be obtained for free by applying to CCDC, 12 Union Road, Cambridge CB2 1EZ, UK, fax: 144-(0) 1223-336033 or e-mail: deposit@ccdc.cam.ac.uk.

4.3. DFT simulation

Compounds **1**, **2a**, **2c**, **3a**, **3b**, **4**, and **5** ground state optimization was conducted using the density functional theory (DFT) method with the B3LYP functional [114,115]. The calculations were performed in the gas phase, and the geometries obtained were confirmed to be true local minima, as no negative frequencies were obtained after the geometry optimization. The results were verified through the absence of negative frequencies after geometry optimization. The HOMO-LUMO energy gap and molecular electrostatic potential (MEP) were calculated using the ground state optimized geometries for additional molecular properties. The DFT calculations were carried out with the Gaussian 16 program suite [116], using the 6-31G(d) basis set for the lighter atoms and the LANL2DZ basis set for Co, including the GD3 empirical dispersion correction [117-121]. The use of Gaussian 16 and the empirical dispersion method ensured that the obtained results were accurate and reliable. For the visualization, the Gaussian16 utility Gaussview was used to generate mapped plots.

4.4. Molecular docking

The molecular docking and studies using the MOE "Molecular Operating Environment" program had been calculated. The fully optimized structures of all complexes have been used for the docking process independently of the DFT part. The molecular docking evaluations were done using the MOE 2019.0102 program. The CIF file from crystallographic data was used without any further optimization except complex **2c**.

In this study, the molecular docking protocol are done between the bimetallic complexes and two different human breast cancer proteins "1HK7: Middle Domain of HSP90 and 3EQM: human placental aromatase cytochrome P450", two different prostate cancers "2Q7K: The androgen receptor prostate Cancer and 2AX6: The androgen receptor" and liver cancer protein (4FM9). The crystal structures of targets prostate cancer proteins (2Q7K and 2AX6) [122,123], breast cancer proteins (1HK7 and 3EQM) [124,125], and liver cancer protein (4FM9) [104]

were retrieved from the Protein Data Bank (<http://www.rcsb.org/pdb/>). All water molecules, ligands and cofactors were removed from the protein structure, and the water molecules around the duplex were also removed, then the hydrogen atoms were added and the protein structure and its charge distribution corrected. The parameters and charges were assigned with MMFF94x force field. After generation, the alpha-site spheres were generated using the site finder module of MOE, and the active site was chosen in the same way as the downloaded structure. The structural model of complexes was docked using the DOCK module of MOE [126,127]. All calculations were carried out on an Intel(R) i7 core (TM), 3.8 GHz based machine running MS Windows 10 as operating system. The docking scoring in MOE software was done utilizing London dG scoring function and has been upgraded using two unrelated refinement methods, auto rotatable bonds were allowed; the best ten binding poses were directed and analyzed to achieve the best score. To compare the docking poses to the ligand in the co-crystallized structure and in order to obtain RMSD of the docking pose, the data base browser was used. The binding free energy and hydrogen bonds between the compounds and amino acids in the receptor were used to rank the binding affinity of the synthesised compounds to the protein molecule. The hydrogen bond was evaluated by measuring the hydrogen bond length, not exceeding the 3.5 Å limit. In addition, the RMSD of the compound position compared to the docking pose was used in ranking. Both RMSD and the mode of interaction of the native ligand within the structure of the receptor were used as standard docked models [128,129]. The validation of the docking method has also been done by using the native ligand, downloaded with protein 2AX6 (Hydroxyflutamide <https://en.wikipedia.org/wiki/Hydroxyflutamide>) and the docking RMSD was 1.35 Å. [130]

CRediT authorship contribution statement

Ahmed Said Mohamed: Writing – original draft, Supervision, Project administration, Investigation, Conceptualization. **Isabelle Jourdain:** Writing – original draft, Investigation, Data curation, Conceptualization. **Michael Knorr:** Writing – review & editing, Writing – original draft, Project administration, Investigation, Conceptualization. **Stephanie Befly:** Data curation. **Abdirahman Elmi:** Data curation. **Farhan Siddique:** Investigation. **Samir Chtita:** Software, Methodology, Formal analysis. **Carsten Strohmann:** Software, Resources, Formal analysis. **Annika Schmidt:** Visualization, Software, Investigation. **Mostafa A. Hussien:** Writing – original draft, Visualization, Software, Formal analysis.

Declaration of competing interest

The authors declare that they have no known competing financial interests or personal relationships that could have appeared to influence the work reported in this paper.

Data availability

Data will be made available on request.

Acknowledgments

This research was funded by the Région Bourgogne-Franche-Comté (DeCOMAB project). We thank the AUF and the UFC for a travel grant for Dr Ahmed Said Mohamed.

Supplementary materials

The following supporting information can be found in the Supplementary Materials: copies of IR(ATR) and NMR spectra of selected compounds **2a**, **3a**, **4** and **5b** (Figs. S1-S6, S8), perspective view of

compound **5a**, Hirshfeld surface analyses of **1**, **3a**, **3c**, and fingerprints plots of **1**, **2a**, **3a**, **3c** (Figs. S9-S15), DFT and MEP data of selected compounds (Figs. S16-S18, Table S3), general X-ray structure analysis (Tables S1-S2), informations related to the studied cancer proteins in the docking studies with selected complexes (Tables S4-S9). Supplementary material associated with this article can be found, in the online version, at ...

Supplementary material associated with this article can be found, in the online version, at [doi:10.1016/j.molstruc.2024.140108](https://doi.org/10.1016/j.molstruc.2024.140108).

References

- [1] C. Zhang, C. Xu, X. Gao, Q. Yao, Platinum-based drugs for cancer therapy and anti-tumor strategies, *Theranostics*. 12 (2022) 2115–2132, <https://doi.org/10.7150/thno.69424>.
- [2] P.J. O'Dwyer, J.P. Stevenson, S.W. Johnson, Clinical Status of Cisplatin, Carboplatin, and Other Platinum-Based Antitumor Drugs, Cisplatin, John Wiley & Sons, Ltd, 1999, pp. 29–69, <https://doi.org/10.1002/9783906390420.ch2>.
- [3] K. Amada. Cobalt: its role in health and disease. In Sigel A, Sigel H, Sigel RK (eds.). Interrelations between Essential Metal Ions and Human Diseases. Metal Ions in Life Sciences. Vol. 13. Springer. pp. 295–320. [doi:10.1007/978-94-007-7500-8_9](https://doi.org/10.1007/978-94-007-7500-8_9).
- [4] M.C. Heffern, N. Yamamoto, R.J. Holbrook, A.L. Eckermann, T.J. Meade, Cobalt derivatives as promising therapeutic agents, *Curr. Opin. Chem. Biol.* 17 (2013) 189–196, <https://doi.org/10.1016/j.cbpa.2012.11.019>.
- [5] A.K. Renfrew, E.S. O'Neill, T.W. Hambley, E.J. New, Harnessing the properties of cobalt coordination complexes for biological application, *Coord. Chem. Rev.* 375 (2018) 221–233, <https://doi.org/10.1016/j.ccr.2017.11.027>.
- [6] D.C. Ware, B.D. Palmer, W.R. Wilson, W.A. Denny, Hypoxia-selective antitumor agents. 7. Metal complexes of aliphatic mustards as a new class of hypoxia-selective cytotoxins. Synthesis and evaluation of cobalt(III) complexes of bidentate mustards, *J. Med. Chem.* 36 (1993) 1839–1846, <https://doi.org/10.1021/jm00065a006>.
- [7] T.W. Failes, C. Cullinane, C.I. Diakos, N. Yamamoto, J.G. Lyons, T.W. Hambley, Studies of a Cobalt(III) complex of the MMP inhibitor marimastat: a potential hypoxia-activated prodrug, *Chem. Eur. J.* 13 (2007) 2974–2982, <https://doi.org/10.1002/chem.200601137>.
- [8] C.R. Munteanu, K. Suntharalingam, Advances in cobalt complexes as anticancer agents, *Dalton. Trans.* 44 (2015) 13796–13808, <https://doi.org/10.1039/C5DT02101D>.
- [9] V. Thamilarasan, N. Sengottuvelan, A. Sudha, P. Srinivasan, G. Chakkaravarthi, Cobalt(III) complexes as potential anticancer agents: Physicochemical, structural, cytotoxic activity and DNA/protein interactions, *J. Photochem. Photobiol. B* 162 (2016) 558–569, <https://doi.org/10.1016/j.jphotobiol.2016.06.024>.
- [10] B. Uprety, R. Chandran, C. Arderne, H. Abrahamse, Anticancer activity of urease mimetic Cobalt (III) complexes on A549-lung cancer cells: targeting the acidic microenvironment, *Pharmaceutics*. 14 (2022) 211, <https://doi.org/10.3390/pharmaceutics14010211>.
- [11] B. Gowdhami, S. Ambika, B. Karthiyayini, V. Ramya, B. Kadalmani, R.T. V. Vimala, M.A. Akbarsha, Potential application of two cobalt (III) Schiff base complexes in cancer chemotherapy: Leads from a study using breast and lung cancer cells, *Toxicol. In Vitro* 75 (2021) 105201, <https://doi.org/10.1016/j.tiv.2021.105201>.
- [12] S. Dasgupta, K. Kar, A. Barua, D. Ghosh, B. Kabi, K. Dewan, A. Chandra, A significantly non-toxic novel Cobalt(III) Schiff base complex induces apoptosis via G2-M cell cycle arrest in human breast cancer cell line MCF-7, *Life Sci.* 308 (2022) 120963, <https://doi.org/10.1016/j.lfs.2022.120963>.
- [13] K. Kar, D. Ghosh, B. Kabi, A. Chandra, A concise review on cobalt Schiff base complexes as anticancer agents, *Polyhedron*. 222 (2022) 115890, <https://doi.org/10.1016/j.poly.2022.115890>.
- [14] D. Schilter, J.M. Camara, M.T. Huynh, S. Hammes-Schiffer, T.B. Rauchfuss, Hydrogenase enzymes and their synthetic models: the role of metal hydrides, *Chem. Rev.* 116 (2016) 8693–8749, <https://doi.org/10.1021/acs.chemrev.6b00180>.
- [15] F. Arrigoni, L. Bertini, L. De Gioia, R. Cingolani, R. Mazzoni, V. Zanotti, G. Zampella, Mechanistic insight into electrocatalytic H₂ production by [Fe₂(CN)₄(μ-CN)(Me)₂](μ-CO)(CO)(Cp)₂]: effects of dithiolate replacement in [FeFe] hydrogenase models, *Inorg. Chem.* 56 (2017) 13852–13864, <https://doi.org/10.1021/acs.inorgchem.7b01954>.
- [16] C. Saviozzi, L. Biancalana, T. Funaioli, M. Bortoluzzi, M. De Franco, M. Guelfi, V. Gandin, F. Marchetti, Triiron complex with N-Ferrocenyl aminocarbyne ligand bridging a diiron core: DFT, electrochemical, and biological insights, *Inorg. Chem.* 63 (2024) 1054–1067, <https://doi.org/10.1021/acs.inorgchem.3c03408>.
- [17] S. Schoch, M. Hadiji, S.A.P. Pereira, M.L.M.F.S. Saraiva, S. Braccini, F. Chiellini, T. Biver, S. Zacchini, G. Pampaloni, P.J. Dyson, F. Marchetti, A Strategy to Conjugate Bioactive Fragments to Cytotoxic Diiron Bis(cyclopentadienyl) Complexes, *Organometallics*. 40 (2021) 2516–2528, <https://doi.org/10.1021/acs.organomet.1c00270>.
- [18] G. Bresciani, J. Vančo, T. Funaioli, S. Zacchini, T. Malina, G. Pampaloni, Z. Dvořák, Z. Trávníček, F. Marchetti, Anticancer Potential of Diruthenium Complexes with Bridging Hydrocarbyl Ligands from Bioactive Alkynols, *Inorg. Chem.* 62 (2023) 15875–15890, <https://doi.org/10.1021/acs.inorgchem.3c01731>.
- [19] M. Odachowski, C. Marschner, B. Blom, A review on 1,1-bis(diphenylphosphino) methane bridged homo- and heterobimetallic complexes for anticancer applications: Synthesis, structure, and cytotoxicity, *Eur. J. Med. Chem.* 204 (2020) 112613, <https://doi.org/10.1016/j.ejmech.2020.112613>.
- [20] M. Haumann, R. Meijboom, J.R. Moss, A. Roodt, Synthesis, crystal structure and hydroformylation activity of triphenylphosphite modified cobalt catalysts, *Dalton. Trans.* (2004) 1679–1686, <https://doi.org/10.1039/B403033H>.
- [21] D. Wang, Y. Lai, P. Wang, X. Leng, J. Xiao, L. Deng, Markovnikov Hydroxylation of Alkynes with Tertiary Silanes Catalyzed by Dinuclear Cobalt Carbonyl Complexes with NHC Ligation, *J. Am. Chem. Soc.* 143 (2021) 12847–12856, <https://doi.org/10.1021/jacs.1c06583>.
- [22] P.L. Pauson, I.U. Khand, Uses of cobalt-carbonyl acetylene complexes in organic synthesis, *Ann. N.Y. Acad. Sci.* 295 (1977) 2–14, <https://doi.org/10.1111/j.1749-6632.1977.tb41819.x>.
- [23] A.M. Hay, W.J. Kerr, G.G. Kirk, D. Middlemiss, Highly Efficient Enantioselective Pauson-Khand Reactions, *Organometallics*. 14 (1995) 4986–4988, <https://doi.org/10.1021/om00011a007>.
- [24] H. Greenfield, H.W. Sternberg, R.A. Friedel, J.H. Wotiz, R. Markby, I. Wender, Acetylenic dicobalt hexacarbonyls. organometallic compounds derived from alkynes and dicobalt octacarbonyl, *J. Am. Chem. Soc.* 78 (1956) 120–124, <https://doi.org/10.1021/ja01582a036>.
- [25] M. Salmain, A. Vessières, P. Brossier, I.S. Butler, G. Jaouen, Carbonylmetalloimmunoassay (CMIA) a new type of non-radioisotopic immunoassay: Principles and application to phenobarbital assay, *J. Immunol. Methods* 148 (1992) 65–75, [https://doi.org/10.1016/0022-1759\(92\)90159-Q](https://doi.org/10.1016/0022-1759(92)90159-Q).
- [26] D. Osella, G. Dutto, G. Jaouen, A. Vessieres, P.R. Raitby, L. De Benedetto, M. J. McGlinchey, Modification of estradiol at the 17-position. Effect of changing the OH group for a transition-metal carbonyl cluster on the estradiol receptor recognition, *Organometallics*. 12 (1993) 4545–4552, <https://doi.org/10.1021/om00035a045>.
- [27] D. Osella, F. Galeotti, G. Cavigliolo, C. Nervi, K.I. Hardcastle, A. Vessières, G. Jaouen, The Hexacarbonyl(ethyne)dicobalt Unit: An Androgen Tag, *Helv. Chim. Acta* 85 (2002) 2918–2925, [https://doi.org/10.1002/1522-2675\(200209\)85:9<2918::AID-HLCA2918>3.0.CO;2-W](https://doi.org/10.1002/1522-2675(200209)85:9<2918::AID-HLCA2918>3.0.CO;2-W).
- [28] I. Ott, K. Schmidt, B. Kircher, P. Schumacher, T. Wiglenda, R. Gust, Antitumor-Active Cobalt–Alkyne Complexes Derived from Acetylsalicylic Acid: Studies on the Mode of Drug Action, *J. Med. Chem.* 48 (2005) 622–629, <https://doi.org/10.1021/jm049326z>.
- [29] I. Jourdain, M. Knorr, T. Charenton, C. Strohmann, J.-L. Kirchhoff, M. Othmann, (μ₂-η⁴-N-(2-Butynyl)phthalimide)(hexacarbonyl)dicobalt, *Molbank*. 2023 (2023) M1545, <https://doi.org/10.3390/M1545>.
- [30] M. Jung, D.E. Kerr, P.D. Senter, Bioorganometallic Chemistry – Synthesis and Antitumor Activity of Cobalt Carbonyl Complexes, *Arch. Pharm. (Weinheim)* 330 (1997) 173–176, <https://doi.org/10.1002/ardp.19973300604>.
- [31] K. Schmidt, M. Jung, R. Keilitz, B. Schnurr, R. Gust, Acetylenhexacarbonyldicobalt complexes, a novel class of antitumor drugs, *Inorg. Chim. Acta* 306 (2000) 6–16, [https://doi.org/10.1016/S0020-1693\(00\)00130](https://doi.org/10.1016/S0020-1693(00)00130).
- [32] I. Ott, B. Kircher, R. Dembinski, R. Gust, Alkyne hexacarbonyl dicobalt complexes in medicinal chemistry and drug development, *Exp. Opin. Ther. Pat.* 18 (2008) 327–337, <https://doi.org/10.1517/13543776.18.3.327>.
- [33] P. Pedrosa, A. Carvalho, P.V. Baptista, A.R. Fernandes, P. Pedrosa, A. Carvalho, P. V. Baptista, A.R. Fernandes, *Inorganic Coordination Chemistry: Where We Stand in Cancer Treatment?* IntechOpen (2018) <https://doi.org/10.5772/intechopen.80233>.
- [34] I. Haiduc, C. Silvestru, Metal compounds in cancer chemotherapy, *Coord. Chem. Rev.* 99 (1990) 253–296, [https://doi.org/10.1016/0010-8545\(90\)80065-2](https://doi.org/10.1016/0010-8545(90)80065-2).
- [35] I. Ott, B. Kircher, C.P. Bagowski, D.H.W. Vleck, E.B. Ott, J. Will, K. Bendsdorf, W. S. Sheldrick, R. Gust, Modulation of the Biological Properties of Aspirin by Formation of a Bioorganometallic Derivative, *Angew. Chem. Int. Ed.* 48 (2009) 1160–1163, <https://doi.org/10.1002/anie.200803347>.
- [36] D. Baecker, J. Sagasser, S. Karaman, A.A. Hormann, R. Gust, Development of methylated cobalt–alkyne complexes with selective cytotoxicity against COX-positive cancer cell lines, *Arch. Pharm. (Weinheim)* 355 (2022), <https://doi.org/10.1002/ardp.202100408>.
- [37] I. Ott, T. Koch, H. Shorafa, Z. Bai, D. Poeckel, D. Steinhilber, R. Gust, Synthesis, cytotoxicity, cellular uptake and influence on eicosanoid metabolism of cobalt–alkyne modified fructoses in comparison to auranofin and the cytotoxic COX inhibitor Co-ASS, *Org. Biomol. Chem.* 3 (2005) 2282–2286, <https://doi.org/10.1039/B504294C>.
- [38] C.D. Sergeant, I. Ott, A. Sniady, S. Meneni, R. Gust, A.L. Rheingold, R. Dembinski, Metallo-nucleosides: synthesis and biological evaluation of hexacarbonyl dicobalt 5-alkynyl-2'-deoxyuridines, *Org. Biomol. Chem.* 6 (2008) 73–80, <https://doi.org/10.1039/B713371E>.
- [39] R. Kaczmarek, D. Korczyński, K. Królewska-Golińska, K.A. Wheeler, F.A. Chavez, A. Mikus, R. Dembinski, Organometallic Nucleosides: Synthesis and Biological Evaluation of Substituted Dicobalt Hexacarbonyl 2'-Deoxy-5-oxopropynyluridines, *ChemistryOpen*. 7 (2018) 237–247, <https://doi.org/10.1002/open.201700168>.
- [40] M.A. Neukamm, A. Pinto, N. Metzler-Nolte, Synthesis and cytotoxicity of a cobaltcarbonyl-alkyne enkephalin bioconjugate, *Chem. Commun.* (2008) 232–234, <https://doi.org/10.1039/B712886J>.

- [41] M. Mori, S.-B. Hyeon, Y. Kimura, A. Suzuki, The Nematicidal Activity of Acetylene Compounds, *Agricultural Biolog. Chem.* 46 (1982) 375, <https://doi.org/10.1080/00021369.1982.10865059>, 22–233.
- [42] T. Steiner, 2-Butyne-1,4-diol, *Acta Cryst C* 52 (1996) 2885–2887, <https://doi.org/10.1107/S0108270196008207>.
- [43] S.M. Oburn, J. Quentin, L.R. MacGillivray, A Divergent Alkyne Diol Directs [2 + 2] Photoreactivity in the Solid State: Cocrystal, Supramolecular Catalysis, and Sublimation Effects, *Molecules*. 24 (2019), <https://doi.org/10.3390/molecules24173059>, 3059–1862.
- [44] U. Rosenthal, G. Oehme, H. Görls, V.V. Burlakov, A.V. Polyakov, A.I. Yanovsky, Yu.T. Struchkov, Crystal and molecular structure of 2-3- η^2 -(butyne-1,4-diol)bis(triisopropylphosphane)nickel(0): (iPr₃P)₂Ni(HOCH₂C≡CCH₂OH)—some peculiarities of the complexation of 2-butyne-1,4-diol with nickel(0) complexes, *J. Organomet. Chem.* 409 (1991) 299–306, [https://doi.org/10.1016/0022-328X\(91\)86155-J](https://doi.org/10.1016/0022-328X(91)86155-J).
- [45] S.S. Shapovalov, A.A. Pasynskii, Yu.V. Torubaev, Complex of bis (triphenylphosphine)platinum(0) with but-2-yne-1,4-diol: Synthesis and molecular structure, *Russ. J. Coord. Chem.* 36 (2010) 801–803, <https://doi.org/10.1134/S1070328410110035>.
- [46] F. Baert, A. Guelzim, P. Coppens, Relation between bonding and the substitution-dependent geometry of a number of dicobalt hexacarbonyl acetylene complexes, *Acta Cryst B* 40 (1984) 590–595, <https://doi.org/10.1107/S0108768184002743>.
- [47] M. Gruselle, B. Malézieux, J. Vaissermann, H. Amouri, A General Route to Prochiral and Chiral Dicationic Molybdenum–Cobalt Acetylenic Complexes: Synthesis, Structures, and Reactivity, *Organometallics*. 17 (1998) 2337–2343, <https://doi.org/10.1021/om971029n>.
- [48] I. Arrais, E. Boccaleri, E. Sappa, A. Secco, Reactions of Co₂(CO)₈(RC≡CR') (RC₂R' = hydroxy- or alkoxy-silyl-alkynes) with tetraethyl-orthosilicate, *J. Sol-Gel Sci. Techn* 38 (2006) 283–292, <https://doi.org/10.1007/s10971-006-6782-7>.
- [49] K.M. Nicholas, Chemistry and synthetic utility of cobalt-complexed propargyl cations, *Acc. Chem. Res.* 20 (1987) 207–214, <https://doi.org/10.1021/ar00138a001>.
- [50] D.D. Díaz, J.P. Ceñal, V.S. Martín, Oxygen-containing 10-, 15-, and 20-membered macrocyclic cobalt complexes from Co₂(CO)₈-bispropargylic alcohol, *Molbank*. 2008 (2008) M562, <https://doi.org/10.3390/M562>.
- [51] A.A. Pasynskii, Y.V. Torubaev, A.Yu Lyakina, R.I. Valiullina, G.G. Aleksandrov, K.A. Lysenko, Synthesis and molecular structures of the dicobalt carbonylphosphine π -complexes containing acetylene with functional groups CH₂OH and CH₂SCMe₃, *Koordinatsionnaya Khimiya* 26 (2000) 112–116.
- [52] F. Carniato, G. Gatti, G. Gervasio, D. Maraballo, E. Sappa, A. Secco, Reactions of Co₂(CO)₈ and of Co₂(CO)₆L (L=3-pentyn-1-ol, 1,4-butyne-diol or 2-methyl-3-butyne-2-ol) with 2(diphenylphosphino)ethyl-triethoxysilane and tris (hydroxymethyl)phosphine for applications to new sol-gel materials, *J. Organomet. Chem.* 694 (2009) 4241–4249, <https://doi.org/10.1016/j.jorganchem.2009.08.040>.
- [53] Y. Gimbert, F. Robert, A. Durif, M.-T. Averbuch, N. Kann, A.E. Greene, Synthesis and characterization of new binuclear Co(0) complexes with diphosphinoamine ligands. a potential approach for asymmetric pauson–khand reactions, *J. Org. Chem.* 64 (1999) 3492–3497, <https://doi.org/10.1021/jo982245o>.
- [54] C.E. Barnes, W.D. King, J.A. Orvis, Cyclopentadienyl cobalt cluster complexes containing the furfuryl ligand, *J. Am. Chem. Soc.* 117 (1995) 1855–1856, <https://doi.org/10.1021/ja00111a034>.
- [55] N.M. Egodawaththa, A.L. Knight, J. Ma, D.A. Knight, E. Guisbert, N. Nesnas, Synthesis and characterization of ligand-stabilized silver nanoparticles and comparative antibacterial activity against *E. coli*, *Int. J. Mol. Sci.* 23 (2022) 15251, <https://doi.org/10.3390/ijms232315251>.
- [56] P.C. Dos Santos, S.M. Mayer, B.M. Barney, L.C. Seefeldt, D.R. Dean, Alkyne Substrate Interaction within the Nitrogenase MoFe Protein, *J. Inorg. Biochem.* 101 (2007) 1642–1648, <https://doi.org/10.1016/j.jinorgbio.2007.05.007>.
- [57] A.S. Mohamed, I. Jourdain, M. Knorr, A. Elmi, S. Chitita, R. Scheel, C. Strohmann, M.A. Hussien, Design of hydroxyl- and thioether-functionalized iron-platinum dimetallacyclopentenone complexes. Crystal and electronic structures, Hirshfeld and docking analyses and anticancer activity evaluated by in silico simulation, *J. Mol. Struct.* 1251 (2022) 131979, <https://doi.org/10.1016/j.molstruc.2021.131979>.
- [58] I. Jourdain, M. Knorr, L. Brieger, C. Strohmann, Synthesis of Tris(arylphosphite)-ligated Cobalt(0) Complexes [Co₂(CO)₆{P(OAr)₃}₂], and their Reactivity towards Phenylacetylene and Diphenylacetylene, *Adv. Chem. Res.* 2 (2020) 1–20, <https://doi.org/10.21926/acr.2004009>.
- [59] C.A. Tolman, Steric effects of phosphorus ligands in organometallic chemistry and homogeneous catalysis, *Chem. Rev.* 77 (1977) 313–348, <https://doi.org/10.1021/cr60307a002>.
- [60] J. Cover, J. Cirera, Computational assessment on the Tolman cone angles for P-ligands, *Dalton. Trans.* 48 (2019) 15036–15048, <https://doi.org/10.1039/C9DT02876E>.
- [61] T. Saito, S. Sawada, ⁵⁹Co Quadrupole Effects on the ¹H, ³¹P, and ⁵⁹Co NMR Spectra of HFeCo₂(CO)₆[P(OCH₃)₃]₂ and the ¹H NMR Spectra of Other Derivatives, *Bull. Chem. Soc. Jpn.* 58 (1985) 459–463, doi.org/10.1246/bc sj.58.459.
- [62] B.E. Hanson, J.S. Manchini, Solution dynamics of (μ -alkyne)Co₂(CO)₄DPM, *Organometallics*. 2 (1983) 126–128, <https://doi.org/10.1021/om00073a023>.
- [63] D.H. Farrar, A.J. Lough, A.J. Poe, T.A. Stromnova, Bis(tricarbonyl(triisopropyl phosphite)-cobalt)(Co-Co) Dichloromethane Solute, *Acta Cryst C51* (1995) 2008–2010, <https://doi.org/10.1107/S0108270195005014>.
- [64] C.J. McAdam, J.J. Brunton, B.H. Robinson, J. Simpson, Ferrocenylethynyl-naphthalenes and acenaphthylenes; communication between ferrocenyl and cluster redox centres, *J. Chem. Soc., Dalton Trans.* (1999) 2487–2495, <https://doi.org/10.1039/A903003D>.
- [65] B. Roufosse, C. Serbu, C. Marschner, S. Prince, B. Blom, Homo and heterometallic complexes containing a group 8 transition metal and μ -diphosphine bridging ligands involved in anticancer research: A review, *Eur. J. Med. Chem.* 274 (2024) 116528, <https://doi.org/10.1016/j.ejmech.2024.116528>.
- [66] D. Pohl, J. Ellermann, M. Moll, F.A. Knoch, W. Bauer, Chemie polyfunktioneller Moleküle. 119 Tetracarbonyl-dicobalt-tetraedran-Komplexe mit den Liganden Bis(diphenyl-phosphanyl)amin, 2-Butin-1,4-diol und tert-Butylphosphaacetylen — Kristallstrukturanalyse des Phosphaalkin-Derivats, *Z. Anorg. Allg. Chem.* 622 (1996) 283–291, <https://doi.org/10.1002/zaac.19966220214>.
- [67] J.-C. Lee, Y.-C. Chang, Y.-J. Ho, K.-M. Chu, H.-L. Chen, F.-E. Hong, Preparation and characterization of cobalt-containing alcohols and diols, *Polyhedron*. 26 (2007) 2987–2996, <https://doi.org/10.1016/j.poly.2007.01.037>.
- [68] S. Clément, L. Guyard, A. Khatyr, M. Knorr, Y. Roussel, M.M. Kubicki, Y. Mugnier, S. Richeter, P. Gerbier, C. Strohmann, Synthesis, crystallographic and electrochemical study of ethynyl[2.2]paracyclophane-derived cobalt metallatetraedranes, *J. Organomet. Chem.* 699 (2012) 56–66, <https://doi.org/10.1016/j.jorganchem.2011.10.034>.
- [69] M. Colapietro, L. Zambonelli, The crystal structure of tetraphenylphosphonium trichloro-(cis-but-2-en-1,4-diol)platinum(II), *Acta Cryst B27* (1971) 734–740, <https://doi.org/10.1107/S056774087100285>.
- [70] V.B. Golovko, M.J. Mays, G.A. Solan, Study of ferrocenyl-substituted Co₂(CO)₆-bispropargylic alcohol complexes as substrates for the formation of chains and macrocycles, *J. Organomet. Chem.* 693 (2008) 2683–2692, <https://doi.org/10.1016/j.jorganchem.2008.05.011>.
- [71] M.J. Went, Synthesis and reactions of polynuclear cobalt-alkyne complexes, *Adv. Organomet. Chem.* 41 (1997) 69–125.
- [72] S.C. Bennett, A. Gelling, M.J. Went, The synthesis of dimetallic thioalkyne complexes of cobalt and molybdenum, *J. Organomet. Chemistry* 439 (1992) 189–199.
- [73] J.H. Van Boom, L. Brandsma, J. F. Arens, Chemistry of acetylenic ethers 82: On the different influence of alkylthio and alkoxy groups on the course of 1,4-Eliminations, *Recl. Trav. Chim. Pays-Bas* 85 (1966) 580–600.
- [74] Q. Gaudillat, A. Krupp, T. Zwingelstein, V. Humblot, C. Strohmann, I. Jourdain, M. Knorr, L. Viau, Silver-based coordination polymers assembled by dithioether ligands: potential antibacterial materials despite received ideas, DOI: 10.1039/d3dt00683b.
- [75] A. Bonnot, M. Knorr, C. Strohmann, C. Golz, D. Fortin, P.D. Harvey, CuX (X = Cl, Br, I) Containing Coordination Polymers Built Upon Isomeric RSCH₂C-CH₂SR (R = p-Tolyl, Benzyl) Dithioether Ligands: First Example of a Luminescent (CuCl)_n/Dithioether Network, *J Inorg Organomet Polym* 25 (2015) 480–494, <https://doi.org/10.1007/s10904-015-0204-7>.
- [76] M.A. Spackman, D. Jayatilaka, Hirshfeld surface analysis, *CrystEngComm*. 11 (2009) 19–32, <https://doi.org/10.1039/B818330A>.
- [77] M.J. Turner, J.J. McKinnon, S.K. Wolff, D.J. Grimwood, P.R. Spackman, D. Jayatilaka, M.A. Spackman, *Crystal Explorer17*, University of Western Australia, 2017, p. 2017.
- [78] J.A. Platts, G.J.S. Evans, M.P. Coogan, J. Overgaard, Electronic structure of the alkyne-bridged dicobalt hexacarbonyl complex Co₂(μ -C₂H₂)(CO)₆: evidence for singlet diradical character and implications for metal–metal bonding, *Inorg. Chem.* 46 (2007) 6291–6298, <https://doi.org/10.1021/ic070278t>.
- [79] M. Yamanaka, E. Nakamura, Density functional studies on the pauson–khand reaction, *J. Am. Chem. Soc.* 123 (2001) 1703–1708, <https://doi.org/10.1021/ja005565>.
- [80] J. Overgaard, H.F. Clausen, J.A. Platts, B. Iversen, Experimental and theoretical charge density study of chemical bonding in a Co dimer complex, *J. Am. Chem. Soc.* 130 (2008) 3834–3843, <https://doi.org/10.1021/ja076152c>.
- [81] M. Harris, S.A. Brusey, A. Moore, Y. Ortin, H. Miller-Bunz, G. Manca, C. Mealli, M. J. McGlinchey, [Co₂(CO)₆(Alkynyl)] complexes of dibenzosuberyl and dibenzosuberenyl carbocations: dibenzotropylium or dibenzoheptafulvene? *Chempluschem*. 81 (2016) 292–306.
- [82] R. Kaczmarek, E. Radzikowska-Cieciura, K. Krolewska-Golińska, R. Dolot, K. A. Wheeler, F.A. Chavez, R. Dembinski, Synthesis and Determination of Anticancer Activity of Dicobalt Hexacarbonyl 2'-Deoxy-5-alkynylfuroprymidines, *ACS Med. Chem. Lett.* 14 (2023) 962–969, <https://doi.org/10.1021/acsmchemlett.3c00152>.
- [83] G.M. Morris, M. Lim-Wilby, Molecular docking, in: A. Kulok (Ed.), *Methods in Molecular Biology*, Humana Press., 2008, pp. 365–382, https://doi.org/10.1007/978-1-59745-177-2_19 (443).
- [84] S.F. Sousa, P.A. Fernandes, M.J. Ramos, Protein-ligand docking: current status and future challenges, *Proteins: Struct., Funct., Bioinf* 65 (1) (2006) 15–26, <https://doi.org/10.1002/prot.21082>.
- [85] D.B. Kitchen, H. Decornez, J.R. Furr, J. Bajorath, Docking and scoring in virtual screening for drug discovery: methods and applications, *Nat. Rev. Drug Discov.* 3 (11) (2004) 935–949, <https://doi.org/10.1038/nrd1549>.
- [86] G. Schneider, H.-J. Böhm, Virtual screening and fast automated docking methods, *Drug Discov. Today* 7 (1) (2002) 64–70, [https://doi.org/10.1016/S1359-6446\(01\)02091-8](https://doi.org/10.1016/S1359-6446(01)02091-8).
- [87] L.G. Ferreira, R.N. Dos Santos, G. Oliva, A.D. Andricopulo, Molecular docking and structure-based drug design strategies, *Molecules*. 20 (7) (2015) 13384–13421, <https://doi.org/10.3390/molecules200713384>.
- [88] E. Lionta, G. Spyrou, D.K. Vassilatis, Z. Cournia, Structure-based virtual screening for drug discovery: principles, applications, and recent advances, *Curr. Top. Med.*

- Chem. 14 (16) (2014) 1923–1938, <https://doi.org/10.2174/1568026614666140929124445>.
- [89] A. Rossi, C. Stagno, A. Piperno, N. Iraci, S. Panseri, M. Montesi, M. Feizi-Dehmayebi, G. Bassi, M.L. Di Pietro, N. Micale, Anticancer activity and morphological analysis of Pt (II) complexes: Their DFT approach, docking simulation, and ADME-Tox profiling, *Appl. Organomet. Chem.* 38 (5) (2024) e7403, <https://doi.org/10.1002/aoc.7403>.
- [90] H.-A. Zahirović, S. Fetahović, M. Feizi-Dehmayebi, R. Bešta-Gajević, M. Dizdar, J. Ostojić, S. Roca, Substituent effect in salicylaldehyde 2-furoic acid hydrazones: Theoretical and experimental insights into DNA/BSA affinity modulation, antimicrobial and antioxidant activity, *J. Mol. Struct.* 1312 (1) (2024) 138628, <https://doi.org/10.1016/j.molstruc.2024.138628>.
- [91] D. Sahin, R.A. Kepecki, M. Feizi-Dehmayebi, S. Akkoc, J.V. Cuevas-Vicario, N. Micale, Biological Activities, DFT Calculations, and Molecular Docking Simulation of Thymol-Based Compounds, *ChemistrySelect.* 9 (2024) e202304572, <https://doi.org/10.1002/slct.202304572>.
- [92] H.-P. Liu, M.-Z. Ren, Z.-J. Quan, X.-C. Wang, Synthesis, structural characterization, molecular docking study, biological activity of carbon monoxide release molecules as potent antitumor agents, *Bioorg. Chem.* 107 (2021) 104621, <https://doi.org/10.1016/j.bioorg.2020.104621>.
- [93] M. Aljohani, Preparation and chemical study on metallic bonding with antibiotics in nanometer form to raise the therapeutic efficiency: structural characterizations of Cu(II), Co(II) and Ni(II) 6-aminopenicillanic acid complexes, *Bull. Chem. Soc. Ethiop.* 37 (1) (2023) 91–100, <https://doi.org/10.4314/bcse.v37i1.8>.
- [94] K. Lofy, Molecular modeling, docking and ADMET of dimethylthiohydantoin derivatives for prostate cancer treatment, *J. Biophys. Chem.* 6 (4) (2015) 91–117, <https://doi.org/10.4236/jbpc.2015.64010>.
- [95] A.S. Basaleh, F.Y. Alomari, A.A. Sharfalddin, N.S. Al-Radadi, D. Domyati, M. A. Hussien, Theoretical investigation by DFT and molecular docking of synthesized oxidovanadium(IV)-based imidazole drug complexes as promising anticancer agents, *Molecules.* 27 (9) (2022) 2796, <https://doi.org/10.3390/molecules27092796>.
- [96] U.A. Çevik, I. Celik, J. Mella, M. Mellado, Y. Özkay, Z.A. Kaplançıklı, Design, Synthesis, and Molecular Modeling Studies of a Novel Benzimidazole as an Aromatase Inhibitor, *ACS. Omega* 7 (2022) 16152–16163, <https://doi.org/10.1021/acsomega.2c01497>.
- [97] N.E. Alshaiikh, M. Zaki, A.A. Sharfalddin, N.S. Al-Radadi, M.A. Hussien, W.M. I. Hassan, Synthesis, structural characterization, DNA/HSA binding, molecular docking and anticancer studies of some D-Luciferin complexes, *Arab. J. Chem.* 16 (7) (2023) 10485, <https://doi.org/10.1016/j.arabjc.2023.104845>.
- [98] A.A. Sharfalddin, A.H. Emwas, M. Jaremko, M.A. Hussien, Transition metal complexes of 6-mercaptopurine: characterization, theoretical calculation, DNA-binding, molecular docking, and anticancer activity, *Appl. Organomet. Chem.* 35 (2021) e6041, <https://doi.org/10.1002/aoc.6041>.
- [99] N.U.Khasanah Ruswanto, G. Ari Wardani, R. Mardianingrum, Synthesis and Computational Study of Bis-(1-(3-Chlorobenzoyl)-3-Phenylthiourea) Cobalt (III) as Anticancer Candidate, *J. Sci. Appl. Chem.* 26 (2023) 238–248, <https://doi.org/10.14710/jksa.26.7.238-248>.
- [100] H. Zhang, T. Yang, Y. Wang, Z. Wang, Z. Zhu, Z. Guo, X. Wang, DNA topoisomerases as additional targets for anticancer monofunctional platinum(II) complexes, *Dalton. Trans.* 50 (2021) 304–310, <https://doi.org/10.1039/D0DT02608E>.
- [101] V.V. D. Rybenkov, C. Ullsperger, A.V. Volodogskii, N.R. Cozzarelli, Simplification of DNA topology below equilibrium values by type II topoisomerases, *Science* (1979) 277 (5326) (August 1997) 690. New York, N.Y.
- [102] D.M. Khaled, M.E. Elshakre, M.A. Noamaan, H. Butt, M.M. Abdel Fattah, D. A. Gaber, A computational QSAR, molecular docking and in vitro cytotoxicity study of novel thioracil-based drugs with anticancer activity against human-DNA topoisomerase II, *Int. J. Mol. Sci.* 23 (2022) 11799, <https://doi.org/10.3390/ijms231911799>.
- [103] A.K. Jadhav, S.M. Karuppaiyil, Molecular docking studies on thirteen fluoroquinolones with human topoisomerase II α and β , *In. Silico Pharmacol.* 5 (2017) 4, <https://doi.org/10.1007/s40203-017-0024-2>.
- [104] T.J. Wendorff, B.H. Schmidt, P. Heslop, C.A. Austin, J.M. Berger, The structure of DNA-bound human topoisomerase II α : conformational mechanisms for coordinating inter-subunit interactions with DNA Cleavage, *J. Mol. Biol.* 424 (2012) 109–124, <https://doi.org/10.1016/j.jmb.2012.07.014>.
- [105] N.M. Hosny, O.A. Ibrahim, A. Belal, M.A. Hussien, M.H. Abdel-Rhman, Synthesis, characterization, DFT, cytotoxicity evaluation and molecular docking of a new carbothioamide ligand and its coordination compounds, *Results. Chem.* 5 (2023) 100776, <https://doi.org/10.1016/j.rchem.2023.100776>.
- [106] M. Chen, D. Sun, J. Li, Z. Wang, H. Liu, L. Pan, H. Chen, Z. Ma, Cobalt(II) terpyridine complexes: synthesis, characterization, antiproliferative activity and molecular docking with proteins and DNA, *New J. Chem.* 47 (2023) 18785–18793, <https://doi.org/10.1039/d3nj03445c>.
- [107] Bruker, APEX3, Bruker AXS Inc., Madison, Wisconsin, USA, 2018.
- [108] Bruker, APEX4, Bruker AXS Inc., Madison, Wisconsin, USA, 2021.
- [109] Bruker, SAINT, Bruker AXS Inc., Madison, Wisconsin, USA, 2012.
- [110] Bruker, SADABS, Bruker AXS Inc., Madison, Wisconsin, USA, 2001.
- [111] O.V. Dolomanov, L.J. Bourhis, R.J. Gildea, J.a.K. Howard, H. Puschmann, OLEX2: a complete structure solution, refinement and analysis program, *J Appl Cryst* 42 (2009) 339–341, <https://doi.org/10.1107/S0021889808042726>.
- [112] G.M. Sheldrick, SHELXT – Integrated space-group and crystal-structure determination, *Acta Cryst A* 71 (2015) 3–8, <https://doi.org/10.1107/S2053273114026370>.
- [113] G.M. Sheldrick, Crystal structure refinement with SHELXL, *Acta Cryst C* 71 (2015) 3–8, <https://doi.org/10.1107/S2053229614024218>.
- [114] A.D. Becke, Density-functional thermochemistry. III. The role of exact exchange, *J. Chem. Phys.* 98 (1993) 5648–5652, <https://doi.org/10.1063/1.464913>.
- [115] C. Lee, W. Yang, R.G. Parr, Development of the Colle-Salvetti correlation-energy formula into a functional of the electron density, *Phys. Rev. B* 37 (1988) 785–789, <https://doi.org/10.1103/PhysRevB.37.785>.
- [116] M.J. Frisch, G.W. Trucks, H.B. Schlegel, G.E. Scuseria, M.A. Robb, J. R. Cheeseman, G. Scalmani, V. Barone, G.A. Petersson, H. Nakatsuji, X. Li, M. Caricato, A.V. Marenich, J.J. Heyd, E.N. Brothers, K.N. Kudin, V.N. Staroverov, T.A. Keith, R. Kobayashi, J. Normand, K. Raghavachari, A.P. Rendell, J.C. Burant, S.S. Iyengar, J. Tomasi, M. Cossi, J.M. Millam, M. Klene, C. Adamo, R. Cammi, J. W. Ochterski, R.L. Martin, K. Morokuma, O. Farkas, J.B. Foresman, D.J. Fox, *Gaussian 16, Revision A.03*, Gaussian, Inc., Wallingford CT, 2016.
- [117] B. Parveen, S. Shahzadi, S. Ali, M. Feizi-Dehmayebi, K.S. Munawar, M. Ashfaq, M. N. Tahir, Synthesis, spectral characterizations, computational studies and biological investigation of 4-(4-(2-hydroxyethyl)phenylamino)-4-oxobutanoic acid and its trimethyltin(IV) complex, *J. Mol. Struct.* 1315 (2024) 138851, <https://doi.org/10.1016/j.molstruc.2024.138851>.
- [118] A. Zahirović, S. Fetahović, M. Feizi-Dehmayebi, A. Višnjevac, R. Bešta-Gajević, A. Kozarić, L. Martić, A. Topčagić, S. Roca, Dual antimicrobial-anticancer potential, hydrolysis, and DNA/BSA binding affinity of a novel water-soluble ruthenium-arene ethylenediamine Schiff base (RAES) *Organometallic, Spectrosc. Acta A* 318 (2024) 124528, <https://doi.org/10.1016/j.saa.2024.124528>.
- [119] A.M. Abu-Dief, O.A. Omran, M. Feizi-Dehmayebi, A. Alqurashi, I. Omar, D. Alhashmialameer, A.D.M. Mohamad, Fabrication, structural elucidation, and DFT calculation of some new hydrophilic metal chelates based on N,N-(1-methyl-2-oxoindolin-3-ylidene)benzohydrazide ligand: Pharmaceutical studies and molecular docking approach, *Appl. Organomet. Chem.* 38 (9) (2024) e7593, <https://doi.org/10.1002/aoc.7593>.
- [120] M.A.E.A. Ali El-Remaily, M.S.H. Alzubi, T. El-Dabea, R.M. El-Khatib, M. S. Kamel, M. Feizi-Dehmayebi, A.M. Abu-Dief, Insights into microwave-promoted synthesis of 3-methyl-4-phenyl-4,9-dihydro-1H-pyrazolo[3,4-d][1,2,4]triazolo [1,5-a]pyrimidine derivatives catalyzed using new Pd (II), Cu (II), VO (II), and Ag (I) complexes as a heterogeneous catalyst and computational studies, *Appl. Organomet. Chem.* 38 (8) (2024) e7587, <https://doi.org/10.1002/aoc.7587>.
- [121] A. Cetin, A. Korkmaz, E. Erdoğan, A. Kösemen, A study on synthesis, optical properties and surface morphological of novel conjugated oligo-pyrazole films, *Mat Chem Phys* 222 (2019) 37–44, <https://doi.org/10.1016/j.matchemphys.2018.09.080>.
- [122] E.B. Askew, R.T. Gampe, T.B. Stanley, J.L. Faggart, E.M. Wilson, Modulation of androgen receptor activation function 2 by testosterone and dihydrotestosterone, *J. Biol. Chem.* 282 (2007) 25801–25816, <https://doi.org/10.1074/jbc.M703268200>.
- [123] C.E. Bohl, D.D. Miller, J. Chen, C.E. Bell, J.T. Dalton, Structural Basis for accommodation of nonsteroidal ligands in the androgen receptor *, *J. Biol. Chem.* 280 (2005) 37747–37754, <https://doi.org/10.1074/jbc.M507464200>.
- [124] P. Meyer, C. Prodromou, B. Hu, C. Vaughan, S.M. Roe, B. Manaretou, P.W. Piper, L.H. Pearl, Structural and functional analysis of the middle segment of Hsp90: implications for ATP hydrolysis and client protein and cochaperone interactions, *Mol. Cell* 11 (2003) 647–658, [https://doi.org/10.1016/S1097-2765\(03\)00065-0](https://doi.org/10.1016/S1097-2765(03)00065-0).
- [125] D. Ghosh, J. Griswold, M. Erman, W. Pangborn, Structural basis for androgen specificity and oestrogen synthesis in human aromatase, *Nature* 457 (2009) 219–223, <https://doi.org/10.1038/nature07614>.
- [126] N.D. Al-Khathami, K.S. Al-Rashdi, B.A. Babgi, M.A. Hussien, M. Nadeem Arshad, N.E. Eltayeb, S.E. Elsilik, J. Lasri, A.S. Basaleh, M. Al-Jahdali, Spectroscopic and biological properties of platinum complexes derived from 2-pyridyl Schiff bases, *J. Saudi Chem. Soc.* 23 (2019) 903–915, <https://doi.org/10.1016/j.jscs.2019.03.004>.
- [127] K.H. Mashat, B.A. Babgi, M.A. Hussien, M. Nadeem Arshad, M.H. Abdellattif, Synthesis, structures, DNA-binding and anticancer activities of some copper(I)-phosphine complexes, *Polyhedron.* 158 (2019) 164–172, <https://doi.org/10.1016/j.poly.2018.10.062>.
- [128] S. Mubarak, M.A. Khanday, A.U.H. Lone, Mathematical analysis based on eigenvalue approach to study liver metastasis disease with applied drug therapy, *Netw Model Anal Health Inform Bioinf.* 9 (2020) 25, <https://doi.org/10.1007/s13721-020-00231-0>.
- [129] P.A. Naik, Modeling the mechanics of calcium regulation in T lymphocyte: a finite element method approach, *Int. J. Biomath.* 13 (2020) 2050038, <https://doi.org/10.1142/S1793524520500382>.
- [130] A. Cetin, A. Donmez, A. Dalar, I. Bildirici, Amino acid and dicyclohexylurea linked pyrazole analogues: synthesis, in silico and in vitro studies, *ChemistrySelect.* 8 (2023) e202204926, <https://doi.org/10.1002/slct.202204926>.